Forschungszentrum Karlsruhe

Technik und Umwelt

Wissenschaftliche Berichte

FZKA 6691

KATRIN – A next generation tritium beta decay experiment with sub-eV sensitivity for the electron neutrino mass

A. Osipowicz[a], H. Blümer[b], G. Drexlin, K. Eitel, G. Meisel, P. Plischke, F. Schwamm, M. Steidl, H. Gemmeke, C. Day, R. Gehring, R. Heller, K.-P. Jüngst, P. Komarek, W. Lehmann, A. Mack, H. Neumann, M. Noe, T. Schneider, L. Dörr, M. Glugla, R. Lässer, T. Kepcija[b], J. Wolf[b], J. Bonn[c], B. Bornschein[c], L. Bornschein[c], B. Flatt[c], C. Kraus[c], B. Müller[c], E.W. Otten[c], J.-P. Schall[c], T. Thümmler[c], C. Weinheimer[c], V. Aseev[d], A. Belesev[d], A. Berlev[d], E. Geraskin[d], A. Golubev[d], O. Kazachenko[d], V. Lobashev[d], N. Titov[d], V. Usanov[d], S. Zadoroghny[d], O. Dragoun[e], A. Kovalik[e], M. Rysavy[e], A. Spalek[e], P.J. Doe[e], S.R. Elliott[f], R.G.H. Robertson[f], J.F. Wilkerson[f]

Institut für Kernphysik

Institut für Prozessdatenverarbeitung und Elektronik

Institut für Technische Physik

Hauptabteilung Versuchstechnik

[a] University of Applied Sciences (FH) Fulda, Marquardtstr. 35, 36039 Fulda, Germany

[b] Universität Karlsruhe (TH), Institut für Experimentelle Kernphysik, Gaedestr. 1, 76128 Karlsruhe, Germany und Institut für Kernphysik, Forschungszentrum Karlsruhe, 76021 Karlsruhe, Germany

[c] Johannes Gutenberg-Universität Mainz, Institut für Physik, 55099 Mainz, Germany

[d] Academy of Sciences of Russia, Institut for Nuclear Research, 60th October Anniversary Prospekt 7a, 117312 Moscow, Russia

[e] Academy of Sciences of the Czech Republic, Nuclear Physics Institute, CZ-250 68 Rez near Prague, Czech Republic

[f] Center for Experimental Nuclear Physics and Astrophysics, and Department of Physics, University of Washington, Seattle, WA 98195, USA

Forschungszentrum Karlsruhe GmbH, Karlsruhe

2001

Impressum der Print-Ausgabe:

Als Manuskript gedruckt

Forschungszentrum Karlsruhe GmbH
Postfach 3640, 76021 Karlsruhe

Mitglied der Hermann von Helmholtz-Gemeinschaft
Deutscher Forschungszentren (HGF)

ISSN 0947-8620

Letter of Intent

KATRIN: A next generation tritium beta decay experiment with sub-eV sensitivity for the electron neutrino mass

A. Osipowicz[a], H. Blümer[b,f], G. Drexlin[b], K. Eitel[b], G. Meisel[b], P. Plischke[b], F. Schwamm[b], M. Steidl[b], H. Gemmeke[c], C. Day[d], R. Gehring[d], R. Heller[d], K.-P. Jüngst[d], P. Komarek[d], W. Lehmann[d], A. Mack[d], H. Neumann[d], M. Noe[d], T. Schneider[d], L. Dörr[e], M. Glugla[e], R. Lässer[e], T. Kepcija[f], J. Wolf[f], J. Bonn[g], B. Bornschein[g], L. Bornschein[g], B. Flatt[g], C. Kraus[g], B. Müller[g], E.W. Otten[g], J.-P. Schall[g], T. Thümmler[g], C. Weinheimer[g], V. Aseev[h], A. Belesev[h], A. Berlev[h], E. Geraskin[h], A. Golubev[h], O. Kazachenko[h], V. Lobashev[h], N. Titov[h], V. Usanov[h], S. Zadoroghny[h], O. Dragoun[i], A. Kovalík[i], M. Ryšavý[i], A. Špalek[i], P.J. Doe[j], S.R. Elliott[j], R.G.H. Robertson[j], J.F. Wilkerson[j]

[a] *University of Applied Sciences (FH) Fulda, Marquardtstr. 35, 36039 Fulda, Germany*

[b] *Forschungszentrum Karlsruhe, Institut für Kernphysik, Postfach 3640, 76021 Karlsruhe, Germany*

[c] *Forschungszentrum Karlsruhe, Institut für Prozessdatenverarbeitung und Elektronik, Postfach 3640, 76021 Karlsruhe, Germany*

[d] *Forschungszentrum Karlsruhe, Institut für Technische Physik, Postfach 3640, 76021 Karlsruhe, Germany*

[e] *Forschungszentrum Karlsruhe, Tritium-Labor Karlsruhe, Postfach 3640, 76021 Karlsruhe, Germany*

[f] *Universität Karlsruhe (TH), Institut für Experimentelle Kernphysik, Gaedestr. 1, 76128 Karlsruhe, Germany*

[g] *Johannes Gutenberg-Universität Mainz, Institut für Physik, 55099 Mainz, Germany*

[h] *Academy of Sciences of Russia, Institute for Nuclear Research, 60$^{\text{th}}$ October Anniversary Prospect 7a, 117312 Moscow, Russia*

[i] *Academy of Sciences of the Czech Republic, Nuclear Physics Institute, CZ-250 68 Řež near Prague, Czech Republic*

[j] *Center for Experimental Nuclear Physics and Astrophysics, and Department of Physics, University of Washington, Seattle, WA 98195, USA*

ABSTRACT

With the compelling evidence for massive neutrinos from recent ν-oscillation experiments, one of the most fundamental tasks of particle physics over the next years will be the determination of the absolute mass scale of neutrinos. The absolute value of ν-masses will have crucial implications for cosmology, astrophysics and particle physics. We present the case for a next generation tritium β decay experiment to perform a high precision direct measurement of the absolute mass of the electron neutrino with sub-eV sensitivity. We discuss the experimental requirements and technical challenges of the proposed Karlsruhe Tritium Neutrino experiment (KATRIN) and outline its physics potential.

KATRIN – Ein Tritium-Betazerfalls-Experiment der nächsten Generation mit sub-eV Empfindlichkeit für die Masse des Elektron-Neutrinos

Zusammenfassung

Neuere Experimente zu Neutrino-Oszillationen haben überzeugend nachgewiesen, dass Neutrinos eine nicht verschwindende Ruhemasse besitzen. Deren Bestimmung wird in den nächsten Jahren eine der wichtigsten Aufgaben der Teilchenphysik sein. Der absolute Wert der Neutrinomasse hat entscheidende Auswirkungen in der Kosmologie, der Astrophysik und der Teilchenphysik. In diesem Report wird ein hochauflösendes Tritium-Betazerfalls-Experiment der nächsten Generation beschrieben, das die Ruhemasse des Elektron-Neutrinos mit einer Empfindlichkeit im sub-eV Bereich messen soll. Es werden die experimentellen Anforderungen und die technischen Herausforderungen des vorgeschlagenen Karlsruhe Tritium Neutrino Experimentes (KATRIN) aufgezeigt. Abschließend wird das physikalische Potential des Experimentes diskutiert.

Contents

1 Introduction

In this paper, we discuss the future of neutrino mass experiments and present a plan for a large tritium β decay experiment with sub-eV sensitivity to the mass of the electron neutrino. The structure of the article is as follows: In the introduction, we report briefly the evidence for neutrino masses, the implications of non-zero neutrino masses for particle physics and cosmology, and discuss several experimental approaches to determine neutrino masses. The current tritium β decay experiments in Mainz/Germany and Troitsk/Russia are described in section 2. In section 3, we present an outline of the proposed future tritium β decay experiment KATRIN.

1.1 Evidences for massive neutrinos

In modern particle physics, one of the most intriguing and most challenging tasks is to discover the rest mass of neutrinos, bearing fundamental implications to particle physics, astrophysics and cosmology. Until recently, the Standard Model (SM) of particle physics assumed neutrinos to be massless. However, actual investigations of neutrinos from the sun and of neutrinos created in the atmosphere by cosmic rays, in particular the recent results of the Super-Kamiokande and SNO experiments [1,2,3], have given strong evidence for massive neutrinos indicated by neutrino oscillations. Neutrino oscillations imply that a neutrino from one specific weak interaction flavor, *e.g.* a muon neutrino ν_μ, transforms into another weak flavor eigenstate, *i.e.* an electron neutrino ν_e or a tau neutrino ν_τ, while travelling from the source to the detector. The existence of neutrino oscillations requires a non-trivial mixing between the weak interaction eigenstates (ν_e, ν_μ, ν_τ) and the corresponding neutrino mass states (ν_1, ν_2, ν_3) and, moreover, that the mass eigenvalues (m_1, m_2, m_3) differ from each other. Consequently, the experimental evidence for neutrino oscillation proves that neutrinos have non-zero masses.

1.2 Implications of neutrino masses

The existence of neutrino oscillations and therefore of neutrino mixing and masses has far-reaching implications to numerous fields of particle physics, astrophysics and cosmology:

- *Particle Physics:*

  The SM of particle physics, which very precisely describes the present experimental data up to the electroweak scale, offers no explanation for the observed pattern of the fermion masses or the mixing among the fermion generations. In particular, it offers no explanation for neutrino masses and neutrino mixing. Accordingly, the recent experimental evidence for neutrino masses and mixing is the first indication for physics beyond the Standard Model.

There are many theories beyond the Standard Model, which explore the origins of neutrino masses and mixings. In these theories, which often work within the framework of Supersymmetry, neutrinos naturally acquire mass. A large group of models makes use of the so-called see-saw effect to generate neutrino masses [4]. Other classes of theories are based on completely different possible origins of neutrino masses, such as radiative corrections arising from an extended Higgs sector [5]. As neutrino masses are much smaller than the masses of the other fermions, the knowledge of the absolute values of neutrino masses is crucial for our understanding of the fermion masses in general. Recently it has been pointed out that the *absolute mass scale of neutrinos* may be even more significant and straightforward for the fundamental theory of fermion masses than the determination of the neutrino mixing angles and CP-violating phases [6]. It will most probably be the absolute mass scale of neutrinos which will determine the scale of new physics.

All these theories extended beyond the SM can be grouped into two different classes, leading either to a hierarchical pattern for the neutrino mass eigenvalues m_i (following the pattern of the quark and charged lepton masses)

$$m_1 \ll m_2 \ll m_3 \tag{1}$$

or resulting in a nearly degenerate pattern of neutrino masses

$$m_1 \approx m_2 \approx m_3 \tag{2}$$

As neutrino oscillation experiments are only sensitive to the differences of the squared masses Δm^2 (*e.g.* $\Delta m^2_{12} = |m_1^2 - m_2^2|$), they cannot measure absolute values of ν masses. While they do not distinguish between the two classes of models, oscillation experiments allow to set a *lower bound* on the absolute ν-mass, as at least one of the neutrino mass eigenvalues should satisfy the inequality:

$$m_i \geq \sqrt{|\Delta m^2|} \tag{3}$$

Analysis of the actual results of Super-Kamiokande [1] in terms of oscillations of atmospheric neutrinos thus gives a lower bound on m_3:

$$m_3 \geq \sqrt{\Delta m^2_{atm}} \sim (0.04 - 0.07)\ \text{eV} \tag{4}$$

However, the fundamental mass scale of neutrinos can be located orders of magnitude above this lower bound (*e.g.* at around 1 eV), as suggested by mass models with degeneracy [8]. Discrimination between hierarchical and degenerate mass scenarios thus requires a sensitivity on the absolute ν-mass scale in the sub-eV range.

Finally, theoretical models come to different conclusions of whether neutrino masses are of the Dirac- or of the Majorana type. A massive neutrino which is

identical to its own antiparticle is called a Majorana particle, while for Dirac-type neutrinos the lepton number distinguishes neutrinos from antineutrinos. This requires the development of experimental techniques for ν-masses in the sub-eV range, which do not depend on assumptions about the Dirac or Majorana character of the neutrino mass.

- *Cosmology and Astrophysics:*

  In astrophysics and cosmology, neutrino masses and mixings play an important role in numerous scenarios, ranging from the formation of light nuclei during the Big Bang nucleosynthesis, the formation and evolution of large scale structures in the universe, up to stellar evolution and the very end of a heavy star, a supernova explosion [10]. Of special interest are the relic neutrinos left over from the Big Bang. The number of these neutrinos in the universe is huge, equivalent to the photons of the Cosmic Microwave Background Radiation (CMBR). The ratio of relic neutrinos to baryons is about 10^9:1, therefore even small neutrino masses are of great importance.

  Thus neutrinos could contribute in a significant way to the large amount of dark matter in the universe. In this context it is important to have in mind that neutrinos act as socalled relativistic or Hot Dark Matter (HDM), whereas other dark matter candidates (supersymmetric particles) represent non-relativistic or Cold Dark Matter (CDM). Cosmological models of structure formation strongly depend on the relative amounts of cold and hot dark matter in the universe, hence a determination of the neutrino HDM contribution to the total dark matter content of the universe would be important for our understanding of structure formation [9].

  Fig. 1 shows the different contributions to the total matter-energy density Ω of the universe, arising from luminous matter, baryons, CDM and the so-called Dark Energy (which is equivalent to the cosmological constant Λ). While the individual contributions of these components are more or less well determined, the contribution Ω_ν of neutrino HDM can vary in the interval $0.003 < \Omega_\nu < 0.25$. The lower bound on Ω_ν arises from the results of Super-Kamiokande on the oscillations of atmospheric neutrinos [1]. The upper bound comes from current tritium β decay experiments [11] and, independently, from recent studies of the evolution of large scale structures in the universe making use of the solar and atmospheric oscillation results [12]. The parameter range of Ω_ν for neutrino HDM, which is presently allowed by experiment, thus spans two orders of magnitude. Clearly, the present situation with regard to Ω_ν is not satisfactory. A determination of Ω_ν or a significant constraint on the allowed parameter range of Ω_ν would lead to a much better understanding of the role of neutrino HDM in the evolution of large scale structures.

  One means of identifying ν HDM and constraining Ω_ν are precise measurements of the temperature fluctuations of the CMBR with balloon or satellite exper-

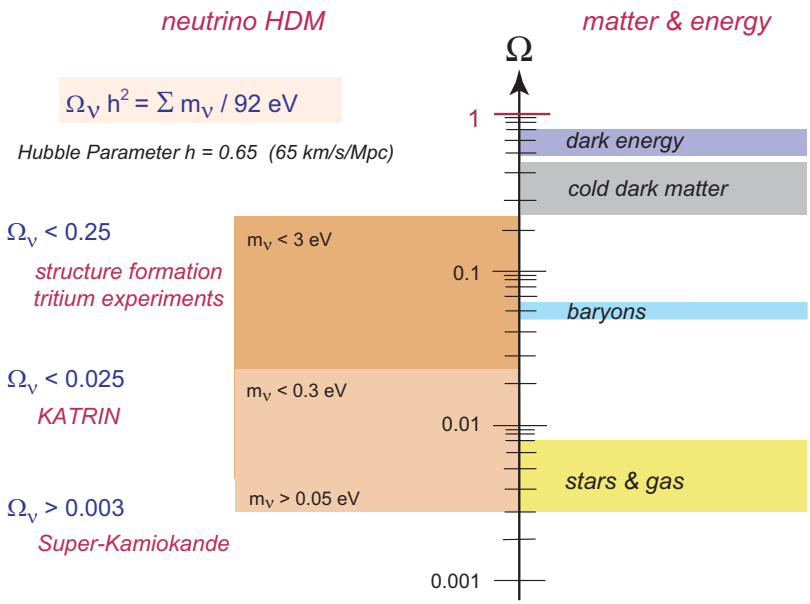

Figure 1: The contribution Ω_ν from neutrino HDM to the total matter energy density Ω of the universe spans two orders of magnitude. The lower bound on Ω_ν comes from the analysis of oscillations of atmospheric ν's. The upper bound stems from current tritium β decay experiments and studies of structure formation. The main motivation of the proposed tritium β decay experiment KATRIN (see section 3) will be to investigate the Ω_ν interval from 0.025-0.25, where the relic neutrinos from the Big Bang would play a significant role as ν HDM in the evolution of large scale structures.

iments. However, the interpretation of these data crucially depends on model assumptions and the precise knowledge of other cosmological parameters. If, on the other hand, the absolute mass scale of neutrinos could be determined with sub-eV precision by a laboratory experiment, the corresponding Ω_ν would be a *fixed* parameter in the analysis of CMBR experiments. This would be especially important for the analysis of high precision CMBR experiments like the recently started MAP [13] satellite and the future PLANCK mission [14].

The investigation of the still open role of neutrino HDM in the evolution of large scale structure is one of the main motivations for the proposed next-generation tritium β decay experiment KATRIN, which is designed to measure the absolute mass of the electron neutrino with sub-eV sensitivity. Correspondingly, KATRIN would be sensitive to a neutrino HDM contribution down to a value of $\Omega_\nu = 0.025$, thus significantly constraining the role of neutrino HDM in structure formation.

As discussed above, the absolute mass scale of neutrinos plays an important role in astrophysics, cosmology and particle physics. While a series of future oscillation experiments using solar [15], reactor [16] and accelerator neutrinos [17,18,19] will improve our understanding of neutrino mixing, the problem of setting the absolute scale of neutrino masses will remain and become a key issue in particle physics.

This absolute mass scale can be inferred by two different experimental approaches: the search for the so-called neutrinoless double β decay and the direct kinematic neutrino mass experiments. Both types of experiments are measuring different neutrino mass parameters and hence are complementary to each other.

1.3 The search for the neutrinoless double β decay

The search for the neutrinoless double β decay ($0\nu\beta\beta$) is a very sensitive means of searching for neutrino masses. The physical process is a twofold β decay in one nucleus at the same time. The normal double β decay with the emission of two electron neutrinos (or electron antineutrinos) $2\nu\beta\beta$ was observed already 14 years ago, but yields no information on the neutrino mass. In the case of the neutrinoless double β decay, the neutrino emitted at one β decay vertex has to be absorbed at the second decay vertex as an antineutrino. This process will only take place on condition that the neutrino is massive and identical to its own antiparticle, *i.e.* it has to be a Majorana particle. Correspondingly, this process violates lepton number conservation by two units.

Up to now, neutrinoless double β decay has not been observed. For the isotope ^{76}Ge, the current best half life limit from the Heidelberg-Moscow experiment results in an upper limit on the effective Majorana mass of the electron neutrino of $m_{ee} < 0.34\,\mathrm{eV}$ at 90% confidence [20]. There are several projects aiming at increasing the sensitivity of $0\nu\beta\beta$ searches into the range of below $0.1\,\mathrm{eV}$ [21]. It is evident that these limits apply only to Majorana neutrino masses and not to Dirac type masses (see sect. 1.5 for the meaning of m_{ee} and its relation to the true neutrino mass scale).

1.4 Direct investigations of the neutrino masses

In contrast to double β decay experiments, direct investigations of the neutrino mass do not rely on further assumptions on the neutrino mass type (Majorana or Dirac). Direct or kinematic experiments can be classified into two categories both making use of the relativistic energy momentum relation $E^2 = p^2c^2 + m^2c^4$ as well as of energy and momentum conservation.

1.4.1 Time-of-flight method

Using a time-of-flight method as a means of measurement of the neutrino masses requires very large distances between source and detector and therefore very intense neutrino sources which only astrophysical, cataclysmic events can provide. The observation of some 20 neutrinos from the Supernova 1987A yielded an upper limit of $m(\nu_e) < 23\,\mathrm{eV}$ [24] by measuring the correlation between the energy and the arrival time of the supernova neutrinos. Though a considerable improvement of the above number can be expected from the measurement of neutrinos from a future,

nearby galactic supernova by large underground neutrino experiments (*e.g.* Super-Kamiokande, SNO), the expected sensitivity will not reach a value below 1 eV [25]. Moreover, the estimated rate of supernova type II explosions is only in the range of one event per several tens of years in our galaxy.

1.4.2 Kinematics of weak decays

The investigation of the kinematics of weak decays is based on the measurement of the charged decay products of weak decays. For the masses of ν_μ and ν_τ the measurement of pion decays into muons and ν_μ at PSI and the investigation of τ-decays into 5 pions and ν_τ at LEP have yielded the upper limits:

$$\begin{aligned} m(\nu_\mu) &< 190 \text{ keV} \quad \text{at } 90\ \% \text{ confidence } [26] \\ m(\nu_\tau) &< 18.2 \text{ MeV} \quad \text{at } 95\ \% \text{ confidence } [27] \end{aligned}$$

Both limits are much larger than the interesting range for cosmology and ν HDM (see fig. 1). However, experiments investigating the mass of the electron neutrino ν_e by analyzing β decays with emission of electrons are providing a sensitivity in the interesting eV-range (see section 2).

1.4.3 Tritium β decay

The most sensitive direct searches for the electron neutrino mass up to now are based on the investigation of the electron spectrum of tritium β decay

$$^3\mathrm{H} \rightarrow {}^3\mathrm{He}^+ + \mathrm{e}^- + \bar{\nu}_e \quad .$$

The electron energy spectrum of tritium β decay for a neutrino with mass m_ν is given by

$$\frac{dN}{dE} = C \times F(Z,E) p E (E_0 - E)[(E_0 - E)^2 - m_\nu^2]^{\frac{1}{2}} \Theta(E_0 - E - m_\nu), \qquad (5)$$

where E denotes the electron energy, p is the electron momentum, E_0 corresponds to the total decay energy, $F(Z,E)$ is the Fermi function, taking into account the Coulomb interaction of the outgoing electron in the final state, the stepfunction $\Theta(E_0 - E - m_\nu)$ ensures energy conservation, and C is given by

$$C = G_F^2 \frac{m_e^5}{2\pi^3} \cos^2\theta_C |M|^2 \ . \qquad (6)$$

Here G_F is the Fermi constant, θ_C is the Cabibbo angle, m_e the mass of the electron and M is the nuclear matrix element. As both M and $F(Z,E)$ are independent of m_ν, the dependence of the spectral shape on m_ν is given by the phase space factor only. In addition, the bound on the neutrino mass from tritium β decay is independent of whether the electron neutrino is a Majorana or a Dirac particle.

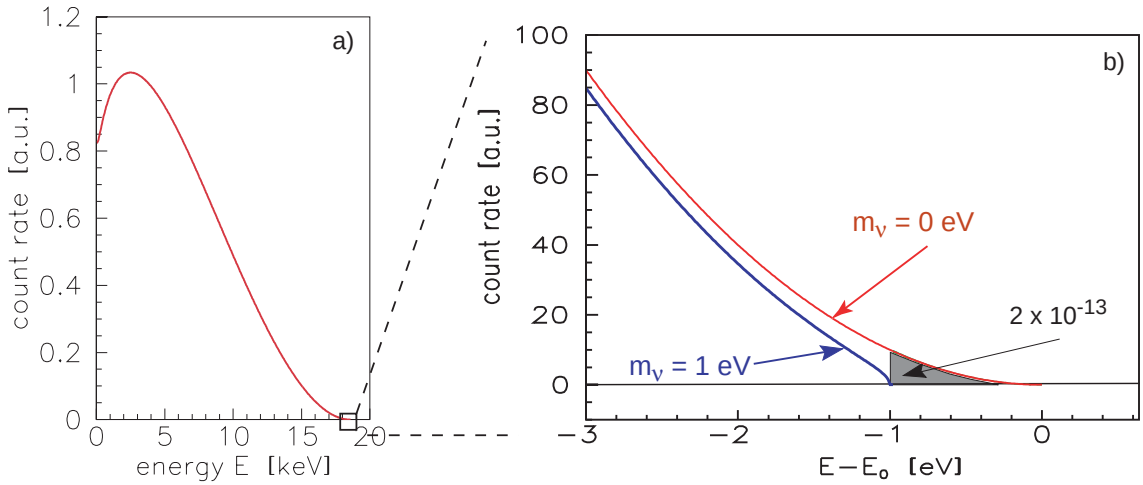

Figure 2: The electron energy spectrum of tritium β decay: (a) complete and (b) narrow region around endpoint E_0. The β spectrum is shown for neutrino masses of 0 and 1 eV.

The signature of an electron neutrino with a mass of m(ν_e)=1 eV is shown in fig. 2 in comparison with the undistorted β spectrum of a massless ν_e. The spectral distortion is statistically significant only in a region close to the β endpoint. This is due to the rapidly rising count rate below the endpoint dN/dE $\propto (E_0-E)^2$. Therefore, only a very narrow region close to the endpoint E_0 is analyzed. As the fraction of β decays in this region is proportional to a factor $(1/E_0)^3$, the very low tritium endpoint energy of 18.6 keV maximizes the fraction of β decays in this region (in fact, tritium has the second lowest endpoint of all β unstable isotopes). Nevertheless, the requirements of tritium β decay experiments with regard to source strength are demanding. As an example, the fraction of β decays falling into the last 1 eV below the endpoint E_0 is only 2×10^{-13} (see fig. 2), hence tritium β decay experiments with high neutrino mass sensitivity require a huge luminosity combined with very high energy resolution.

Apart from offering a low endpoint energy E_0 and a moderate half life of 12.3 y, tritium has further advantages as β emitter in ν mass investigations:

1. the hydrogen isotope tritium and its daughter, the $^3He^+$ ion, have a simple electron shell configuration. Atomic corrections for the β decaying atom -or molecule- and corrections due to the interaction of the outgoing β electron with the tritium source can be calculated in a simple and straightforward manner

2. The tritium β decay is a super-allowed nuclear transition. Therefore, no corrections from the nuclear transition matrix elements M have to be taken into account.

The combination of all these features makes tritium an almost ideal β emitter for neutrino mass investigations.

1.4.4 Other approaches to β decay

A different approach to directly measure the electron neutrino mass is the use of cryogenic bolometers. In this case, the β source can be identical to the β electron spectrometer. This new technique has been applied to the isotope ^{187}Re, which has a 7 times lower endpoint energy than tritium[28]. The experiments are still in the early stage of development. Current microcalorimeters reach an energy resolution of $\Delta E \sim 5\,\mathrm{eV}$ for short-term measurements and yield an upper limit of $m(\nu_e) < 26\,\mathrm{eV}$ [29]. To further improve the statistical accuracy, the principle of integration of active source and detector requires the operation of large arrays of microcalorimeters. The expected sensitivity on the neutrino mass in the nearer future will be below $\sim 10\,\mathrm{eV}$ [29].

1.5 Neutrino mixing and mass scale

The effects of neutrino mixing on tritium β decay and $0\nu\beta\beta$ experiments can be significant. Below we discuss the implications of ν-mixing in the determination of the absolute mass scale of neutrinos for both experimental approaches, following largely the discussions in [6,7].

1.5.1 Mixing and $0\nu\beta\beta$

Considering neutrino mixing for $0\nu\beta\beta$ decay, the *effective* Majorana mass m_{ee} is a coherent sum of all neutrino mass states ν_i contributing to the electron neutrino ν_e. The parameter m_{ee} is a combination of mass eigenvalues m_i, Majorana phases and mixing parameters given by

$$m_{ee} = \left| \sum_{i=1}^{3} U_{ei}^2 \cdot m_i \right| \tag{7}$$

Since the Majorana CP-phases are unknown, strong cancellations in the sum over all neutrino states ν_i can occur.

1.5.2 Mixing and tritium β decay

In the case of tritium β decay, the presence of mixing modifies eq. (5) to:

$$\frac{dN}{dE} = C \times F(Z,E) pE (E_0 - E) \sum_i |U_{ei}|^2 [(E_0 - E)^2 - {m_i}^2]^{\frac{1}{2}} \Theta(E_0 - E - m_i), \tag{8}$$

The step function, $\Theta(E_0 - E - m_i)$, ensures that a neutrino state ν_i is only produced if the energy available is larger than its mass. In general, the effects of mixing will lead to the following spectral modifications :

1. the β spectrum ends at $E_{0'} = E_0 - m_1$, where m_1 is the lightest mass in the neutrino mass spectrum (i.e. the electron spectrum bends at $E \lesssim E_{0'}$)

2. the appearance of 'kinks' at the electron energy $E_e^i \approx E_0 - m_i$, with the size of the kinks being determined by the mixing elements $|U_{ei}|^2$.

For general mixing schemes with 3 neutrinos (3ν) or 3 active neutrinos and 1 'sterile' (4ν), the spectral shape of tritium β decay can be rather complex, requiring the introduction of at least five independent parameters (two mixing parameters and three masses for 3ν-mixing). In [6,7] all possible 3ν or 4ν mixing schemes (with normal or inverted mass hierarchy) have been discussed extensively. In the following, we restrict our discussion to the schemes explaining the solar and atmospheric neutrino oscillation data. This omits the 4ν schemes incorporating the LSND oscillation results [22], which, however, have not been confirmed by other experiments such as KARMEN [23].

If the pattern of neutrino masses is hierarchical ($m_1 \ll m_2 \ll m_3$), the largest mass, $m_3 \simeq \sqrt{\Delta m^2_{atm}} = (4-7)\times 10^{-2}$ eV, would be too small to be observed in tritium β decay. For models of quasi-degenerate neutrino masses with an absolute mass scale in the range of sensitivity of future tritium β experiments, the effects of non-zero ν-masses and mixings reduce to a single parameter, $m^2(\nu_e)$. With $m_1 \approx m_2 \approx m_3$, the only distortion of the spectrum to be seen is a bending at the electron energy $E_0 - m(\nu_e)$, equivalent to the case of a ν_e with definite mass and no mixing. Therefore the analysis of the β spectrum can be parametrized by

$$m^2(\nu_e) = \sum_{i=1}^{3} |U_{ei}|^2 \cdot m_i^2 \quad . \tag{9}$$

In contrast to eq. (7), here the absolute values of the squared mixing matrix elements are involved. Therefore the sum contains only non-negative elements, no cancellations can happen. Hence, the neutrino mass $m(\nu_e)$ extracted from the experiment fixes the absolute mass scale ($m_1 \approx m_2 \approx m_3$), taking into account the small values of Δm^2 from oscillation experiments.

1.5.3 Absolute neutrino mass scale

While tritium β decay and $0\nu\beta\beta$ are largely complementary to each other, it is nevertheless interesting to compare the two parameters $m(\nu_e)$ and m_{ee} with each other (assuming neutrinos are Majorana particles) and to investigate their relation to the fundamental neutrino mass scale in the presence of ν-mixing. For a 3ν mixing the following bounds on the β decay mass $m(\nu_e)$ can be derived:

$$m_{ee} < m(\nu_e) < \frac{m_{ee}}{|| \cos 2\theta_\odot | (1 - |U_{e3}|^2) - |U_{e3}|^2 |}, \tag{10}$$

The ν_e mixing parameters in (10) can be deduced from the results of oscillation experiments using solar neutrinos (solar mixing angle $\theta_\odot$) and reactor antineutrinos ($|U_{e3}|^2$).

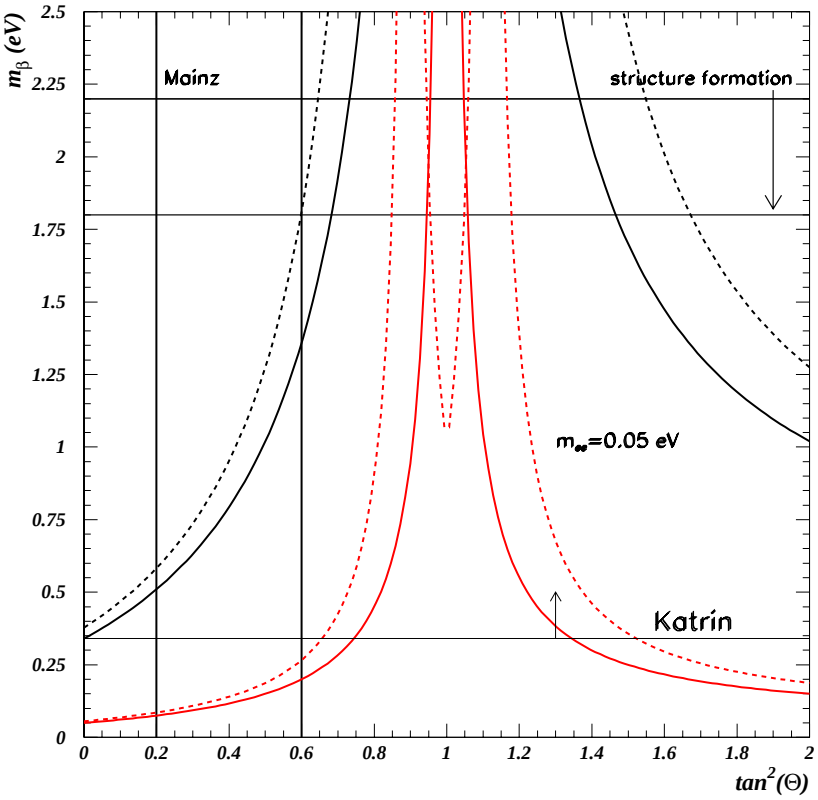

Figure 3: Bounds on the effective β decay mass $m(\nu_e)$ (= m_β in ref. [6]) as functions of the solar mixing angle $\theta_\odot$ (for 3ν mixing models with strong mass degeneracy). The horizontal lines correspond to the current and the proposed future tritium β decay experiments (Mainz and KATRIN) as well as to structure formation. For results from $0\nu\beta\beta$ experiments, which strongly depend on $\theta_\odot$, the upper solid (dashed) line corresponds to the present bound $m_{ee} \leq 0.34\,\mathrm{eV}$ and $|U_{e3}|^2 = 0$ ($|U_{e3}|^2$=0.05), the lower solid (dashed) line corresponds to an envisaged future limit of $m_{ee} \leq 0.05\,\mathrm{eV}$ and $|U_{e3}|^2 = 0$ ($|U_{e3}|^2$=0.05). The vertical lines mark the current 90 % C.L. borders of the large mixing angle (LMA) solution region for solar ν's. (fig. taken from ref. [6])

Fig. 3 shows the bounds on $m(\nu_e)$ from current and future tritium β decay and $0\nu\beta\beta$ experiments as a function of the solar mixing angle $\theta_\odot$ for two different values of $|U_{e3}|^2$. It is interesting to note that for large values of $\theta_\odot$ a positive signal from $0\nu\beta\beta$ experiments only yields a *lower limit* on the fundamental neutrino mass scale. The relationship between m_{ee} and the 'true' mass scale $m(\nu_e)$ depends crucially on the solar mixing parameter $\theta_\odot$. The weakest $0\nu\beta\beta$ bounds on $m(\nu_e)$ appear at maximum mixing of solar neutrinos $\tan^2\theta_\odot = 1$ (for $|U_{e3}|^2$=0). The actual allowed parameter spaces for $\theta_\odot$ from solar neutrino experiments (including the recent SNO results) have been evaluated in [30]. While small solar mixing angles $\tan^2\theta_\odot < 0.01$ (so-called SMA solutions) are disfavored by current results, solutions with large mixing angle $\tan^2\theta_\odot > 0.1$ (either the socalled LMA or LOW solutions) are strongly favored.

This implies that the absolute ν-mass scale cannot easily be restored from m_{ee} due to possible cancellations depending on the unknown CP-violating phases. Moreover, there are uncertainties in the calculations of the nuclear matrix elements of $0\nu\beta\beta$ transitions, which may lead to systematic errors in the relation between m_{ee} and the true mass scale. Finally, many other exchange modes apart from light Majorana particles can contribute to the $0\nu\beta\beta$ transition rate [31], thereby adding further uncertainties. Thus the development of direct methods of determination of the neutrino mass is essential for a complete reconstruction of the neutrino mass spectrum.

2 Tritium β decay experiments

The almost ideal features of tritium as a β emitter have been the reason for a long series of tritium β decay experiments. Figure 4 shows the evolution on the observable m_ν^2 of the various tritium β decay experiments over the last decade. It is remarkable that the error bars on m_ν^2 have decreased by nearly two orders of magnitude. Equally important is the fact that the problem of negative values for m_ν^2 of the early nineties has disappeared due to better understanding of systematics and improvements in the experimental setups.

2.1 MAC-E-Filter

The high sensitivity of the Troitsk and the Mainz neutrino mass experiments is due to a new type of spectrometers, so-called MAC-E-Filters (Magnetic Adiabatic Collimation combined with an Electrostatic Filter). This new type was first proposed in [32]. Later this method was reinvented specifically for the search for the electron neutrino mass at Troitsk and Mainz, independently. It combines high luminosity and low background with a high energy resolution, both essential to measure the neutrino mass from the endpoint region of a β decay spectrum.

The main features of the MAC-E-Filter are illustrated in fig. 5(a). Two superconducting solenoids are producing a magnetic guiding field. The β electrons, which are starting from the tritium source in the left solenoid into the forward hemisphere, are

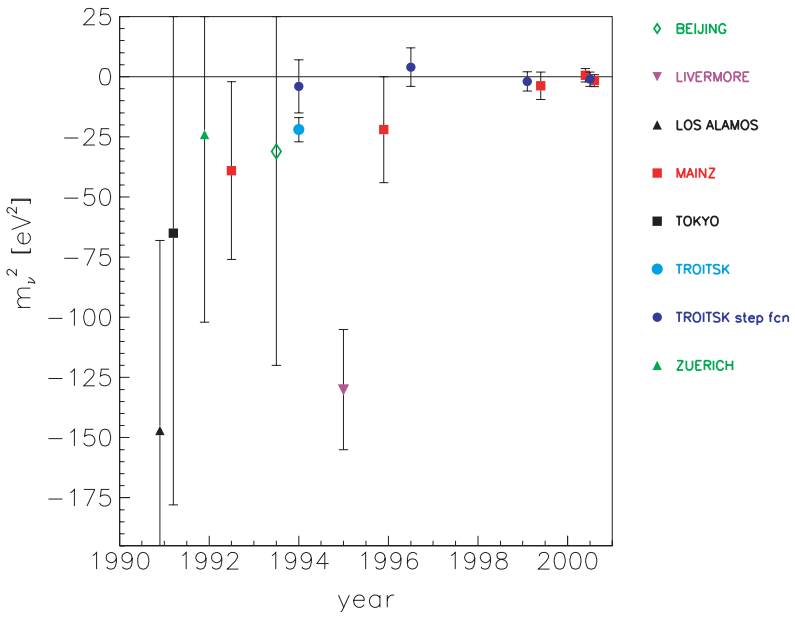

Figure 4: Results of tritium β decay experiments on the observable m_ν^2 over the last decade. The experiments at Los Alamos, Zürich, Tokyo, Beijing and Livermore [33,34,35,68,36] used magnetic spectrometers, the experiments at Troitsk and Mainz [37,38] are using electrostatic spectrometers of the MAC-E-Filter type (see text).

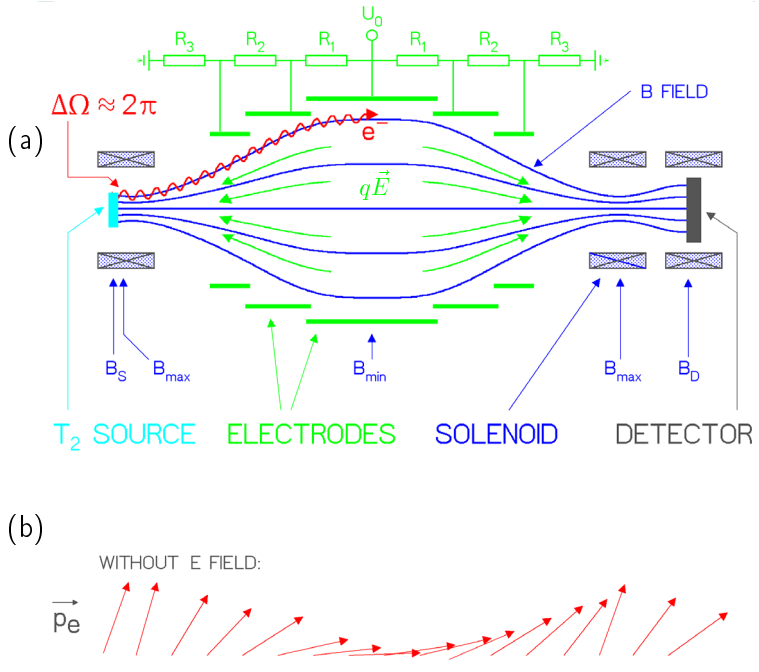

Figure 5: Principle of the MAC-E-Filter. (a) Experimental setup, (b) Momentum transformation due to adiabatic invariance of magnetic orbit momentum μ in the inhomogeneous magnetic field.

guided magnetically on a cyclotron motion around the magnetic field lines into the spectrometer, thus resulting in an accepted solid angle of up to 2π. On their way into the center of the spectrometer the magnetic field B drops by many orders of magnitude. Therefore, the magnetic gradient force transforms most of the cyclotron energy $E_\perp$ into longitudinal motion. This is illustrated in fig. 5(b) by a momentum vector. Due to the slowly varying magnetic field the momentum transforms adiabatically, therefore the magnetic moment μ keeps constant (equation given in non-relativistic approximation):

$$\mu = \frac{E_\perp}{B} = const. \tag{11}$$

This transformation can be summarized as follows: The β electrons, isotropically emitted at the source, are transformed into a broad beam of electrons flying almost parallel to the magnetic field lines.

This parallel beam of electrons is running against an electrostatic potential formed by a system of cylindrical electrodes. All electrons with enough energy to pass the electrostatic barrier are reaccelerated and collimated onto a detector, all others are reflected. Therefore the spectrometer acts as an integrating high-energy pass filter. The relative sharpness $\Delta E/E$ of this filter is given by the ratio of the minimum magnetic field B_A in the center plane and the maximum magnetic field B_{max} between β electron source and spectrometer :

$$\frac{\Delta E}{E} = \frac{B_A}{B_{max}} \quad . \tag{12}$$

Varying the electrostatic retarding potential allows to measure the β spectrum in an integrating mode.

In order to suppress electrons which have a very long path within the tritium source and therefore possess a high scattering probability, the electron source is placed in a magnetic field B_S (see fig. 5), which is lower than the maximum magnetic field $B_{\max}$. This restricts the maximum accepted starting angle of the electrons $\theta_{\max}$ by the magnetic mirror effect to:

$$\sin\theta_{\max} = \sqrt{\frac{B_{\mathrm{S}}}{B_{\max}}} \tag{13}$$

2.2 The Mainz and the Troitsk experiments

The experiments at Troitsk [37] and Mainz [38] are using similar MAC-E-Filters differing somewhat in size: The diameter and length of the Mainz (Troitsk) spectrometers are 1 m (1.5 m) and 4 m (7 m). The major differences between the two setups are the tritium sources.

The Troitsk experiment uses a windowless gaseous tritium source (WGTS) which is based on the adiabatic transport of electrons in a strong longitudinal magnetic field and circulation of tritium gas at low pressure by means of a differential pumping

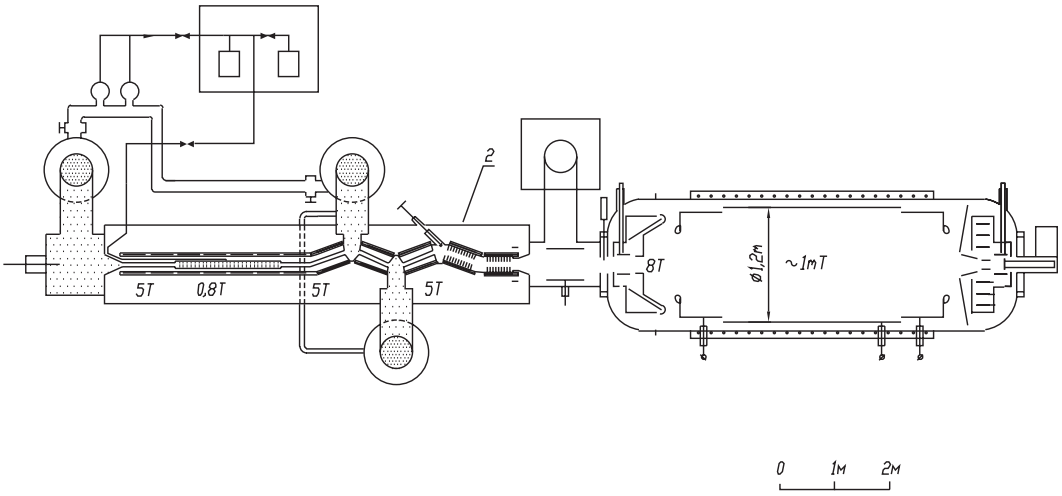

Figure 6: Schematic view of the Troitsk experimental setup [43)].

system [39)] (see fig. 6). This approach was first pioneered in an experiment at Los Alamos [33)]. An essential refinement made at Troitsk was the use of a strong magnetic field for electron transport. This technique permits to use multiple bends of the transport channel, thus providing better differential pumping and smooth coupling to the MAC-E-Filter spectrometer. The Troitsk WGTS (a 3 m long tube of 50 mm diameter filled with 0.01 mbar of T_2) provides a number of beneficial features for the study of the tritium β spectrum, such as guaranteed homogeneity over the cross section of the source and reliable on-line control of inelastic energy losses of electrons in the source. It further allows to use theoretical calculations of free molecular final state corrections and almost totally suppresses back scattering.

Mainz uses a film of molecular tritium quench-condensed onto a substrate of highly oriented pyrolytic graphite. The film has a diameter of 17 mm and a typical thickness of 40 nm, which is measured by laser ellipsometry. In the years 1995–1997 the Mainz setup was upgraded to enhance the count rate and to decrease the background rate. As second substantial improvement a new cryostat now provides temperatures of the tritium film below 2 K to avoid a roughening transition of the film, which was a source of systematic errors of earlier Mainz measurements. The roughening process is a temperature activated surface diffusion process, therefore low temperatures are necessary to get time constants much longer than the duration of the measurement [41,42)]. The full automation of the apparatus and remote control allows to perform long term measurements over several months per year. Figure 7 gives a sketch of the Mainz setup. Since this upgrade, the count rate, background and energy resolution of the Mainz setup are about the same as the ones of the Troitsk experiment.

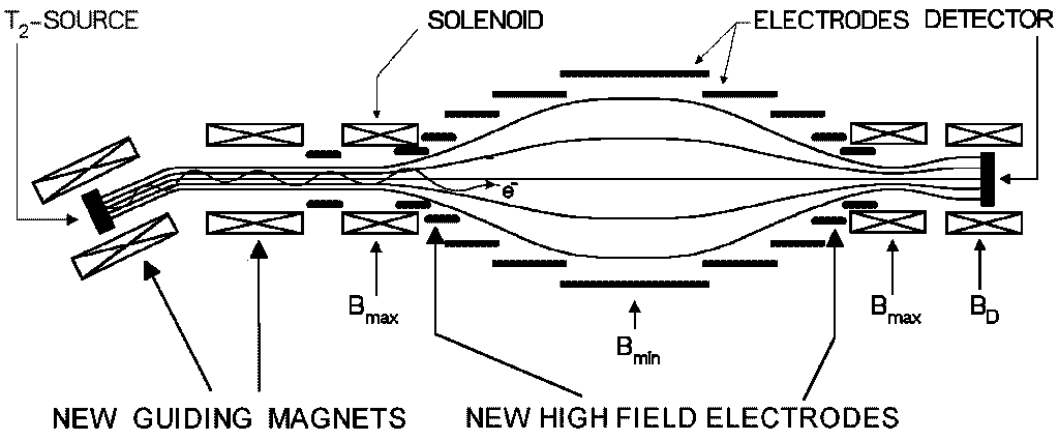

Figure 7: The upgraded and improved Mainz setup (schematically, not in realistic scale). The outer diameter amounts to 1 m, the distance from the source to the detector is 6 m [38].

2.3 Results of the Troitsk Neutrino Mass Experiment

The Troitsk experiment has taken tritium data for 200 days from 1994 on. Since the first measurements, the Troitsk experiment has observed a small anomaly in the energy spectrum, located a few eV below the β endpoint E_0. The distortion resembles sharp step of the count rate [43]. Since a MAC-E-Filter is integrating, a sharp step corresponds to a narrow line in the primary spectrum. The data indicate a relative intensity of about 10^{-10} of the total decay rate. From 1998 on, the Troitsk group reported that the position of this line seems to oscillate with a frequency of 0.5 years between 5 eV and 15 eV below E_0 [37]. The cause for such an anomaly is not known. Detailed investigations as well as synchronous measurements with the Mainz experiment are under way and will help to clarify this effect.

Fitting a standard β spectrum to the Troitsk data results in significantly negative values of $m(\nu_e)^2 \approx -10$ to -20 eV^2. However, describing the anomaly phenomenologically by adding a monoenergetic line with free amplitude and position to a standard β spectrum results in values of m_ν^2 compatible with zero. The average over all Troitsk runs until 1999 then amounts to [44]

$$m(\nu_e)^2 = (\,-1.0 \pm 3.0 \pm 2.5\,)\ eV^2$$

which corresponds to an upper limit of

$$m(\nu_e) \leq 2.5\ eV^2 \qquad (95\ \%\ \text{C.L.})$$

2.4 Results of the Mainz Neutrino Mass Experiment

Figure 8 shows the endpoint region of the Mainz 1998 and 1999 data in comparison with the former Mainz 1994 data. An improvement of the signal-to-background ratio

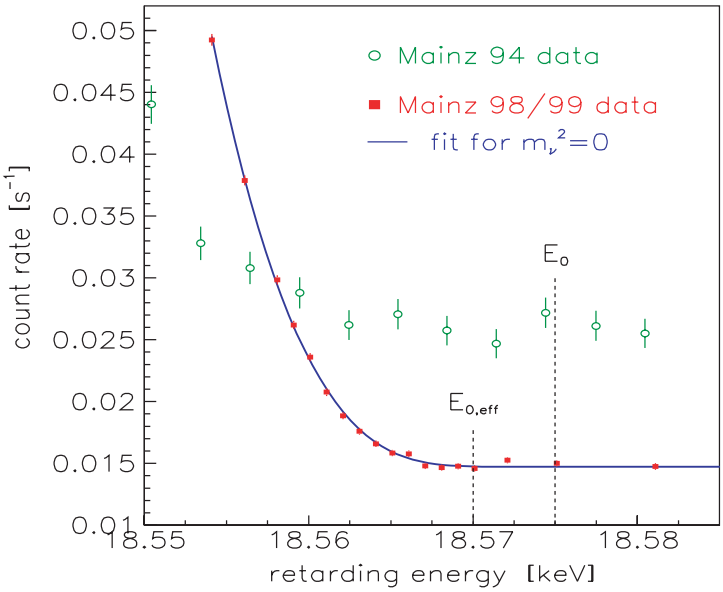

Figure 8: Averaged count rate of the Mainz 1998 and 1999 data (points) with fit (line) in comparison with previous Mainz data from 1994 [45] as function of the retarding energy near the endpoint E_0, and effective endpoint $E_{0,\mathrm{eff}}$. The position of the latter takes into account the width of response function of the setup and the mean rotation-vibration excitation energy of the electronic ground state of the $^3HeT^+$ daughter molecule.

by a factor 10 as well as a significant enhancement of the statistical quality of the data is clearly visible. The main systematic uncertainties of the Mainz experiment are originating from the physics and the properties of the quench-condensed tritium film and originate from the inelastic scattering of β electrons within the tritium film, the excitation of neighbor molecules due to the β decay, and the self-charging of the tritium film by its radioactivity. As a result of detailed investigations [46,47,48], these systematic uncertainties were reduced significantly.

The data of the last runs of 1998 and 1999 (see fig. 8) neither show a Troitsk-like anomaly nor any other residual problem. The most sensitive analysis on the neutrino mass, in which only the last 70 eV of the β spectrum below the endpoint are used results in

$$m(\nu_e)^2 = (\,-1.6 \pm 2.5 \pm 2.1\,)\ eV^2$$

which is compatible with a zero neutrino mass and corresponds to an upper limit on the electron neutrino mass of:

$$m(\nu_e) \leq 2.2\ eV \qquad (95\ \%\ \mathrm{C.L.}) \quad .$$

The analysis of the new Mainz 1998 and 1999 data [49] improved the published former upper limit of $m(\nu_e) < 2.8\,\mathrm{eV}$ [38], which was based on the Mainz 1998 data alone. Together with the Troitsk results, they represent the world's best sensitivity on a neutrino mass in a direct neutrino mass experiment.

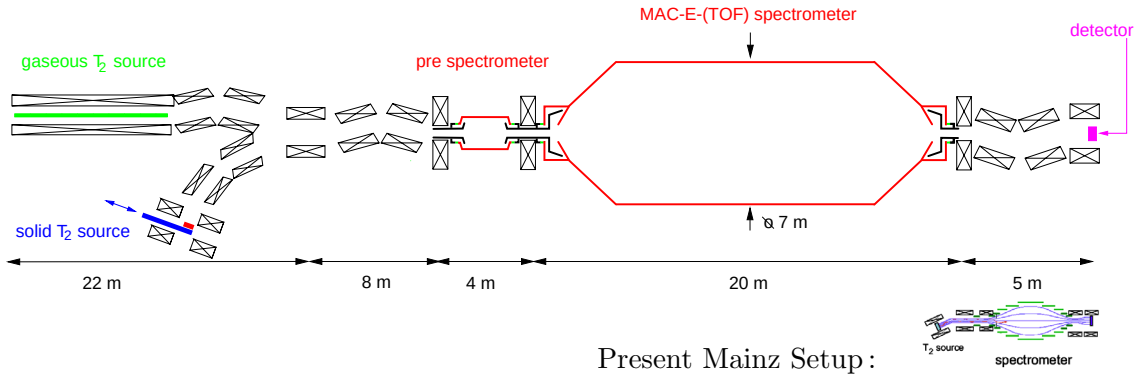

Figure 9: Schematic view of the proposed next-generation tritium β decay experiment KATRIN. The main components of the system comprise a windowless gaseous tritium source (WGTS), a quench condensed tritium source (QCTS), a pre-spectrometer and a large electrostatic spectrometer of 7 m diameter and 20 m length with an energy resolution of 1 eV. An electron transport system guides electrons from the T_2 sources to the spectrometers, while eliminating all tritium molecules in a two stage process, consisting of a differential pumping part followed by a cryotrapping part The pre-spectrometer having a retarding potential of about 100 V below the β endpoint allows only the high energy tail of the β electrons, comprising about 2×10^{-7} of the total decay rate, to enter the main spectrometer. The overall length of this linear set-up amounts to about 70 m. Shown for comparison is the present Mainz setup at the same scale.

3 The KATRIN experiment

The tritium β decay experiments at Troitsk and Mainz have almost reached their limit of sensitivity. It can be estimated that future measurements of both experiments would improve the current limit only marginally to $m(\nu_e) < 2\,\mathrm{eV}$. To measure an electron neutrino mass in the sub-eV region thus requires a new experiment with much higher ν-mass sensitivity.

In the following sections we present a design study for a next-generation tritium β decay experiment with a sensitivity to sub-eV neutrino masses, following first ideas presented in [47,50]. The experiment we propose, the Karlsruhe Tritium Neutrino (KATRIN) experiment, would have an estimated sensitivity of $m(\nu_e) = 0.35\,\mathrm{eV}$ (90 % C.L.), which is about one order of magnitude better than the sensitivity of the current experiments. For $m^2(\nu_e)$, which is the observable in a direct neutrino mass measurement, this corresponds to an improvement by two orders of magnitude. This requires significant improvements of the tritium source strength and the spectrometer resolution.

The proposed KATRIN set-up is based on the long-term experience with the existing spectrometers of the MAC-E type [39,40] and has been prepared by groups from Fulda, Karlsruhe, Mainz, Prague, Seattle and Troitsk.

3.1 Experimental overview

A schematic view of the proposed experimental configuration is shown in fig. 9. It can be grouped into four functional units:

- the two molecular tritium sources WGTS and QCTS (including tritium supply and handling)
- the electron transport and tritium elimination line (comprising the differential pumping and cryotrapping sections)
- the electrostatic pre- and main-spectrometer
- the β electron detector

In order to reach a sub-eV sensitivity, an energy resolution of $\Delta E = 1$ eV is necessary at the tritium β decay endpoint of 18.6 keV, implying a ratio of magnetic fields $B_{\min} / B_{\max} = 5 \times 10^{-5}$. This resolution would correspond to an improvement of a *factor of 4* compared to the experiments in Troitsk and Mainz. Since the energy interval of interest below the endpoint E_0 (see fig. 2) rapidly decreases with smaller neutrino mass m_ν, the signal rate has to be increased. This can be achieved by a higher T_2 source strength corresponding to a larger source area A_S and a higher and optimized column density ρd. Subsequently, this requires a larger area of the analyzing plane A_A of the spectrometer. To meet these demands, a large electrostatic spectrometer with an analyzing plane of 7 m diameter and a T_2 source with effective cross section of $A_{S,\text{eff}} \approx 16$ cm^2 and column density of $(\rho d)_{\text{eff}} \approx 5 \cdot 10^{17}$ molecules/cm^2 are considered for KATRIN.

In addition, a low background count rate of the order of 10^{-2} counts/s or less at the tritium β-decay endpoint region at 18.6 keV is required when looking for sub-eV neutrino mass effects. Among the various background processes, the ionization of residual gas molecules as well as the decay of any residual tritium in the spectrometer play an important role. Therefore, the low background count rate is implying stringent requirements on the vacuum conditions of the electrostatic spectrometers. To further reduce the background in the main spectrometer, a pre-spectrometer (located between the tritium source and the main-spectrometer) will act as a pre-filter at a retarding energy of order of 100 eV below the β endpoint E_0, reducing the amount of β electrons entering the main-spectrometer by about 7 orders of magnitude. Suppression of cosmogenic background finally calls for a state-of-the-art detector with good energy- and spatial resolution for low energy electrons in the keV range.

During the longterm tritium measurements special emphasis will be put on the control of all systematic effects which might influence the experimental results. As the most important systematic effects are associated with the properties of the tritium source, two independent tritium sources with different systematics are proposed for KATRIN: a windowless gaseous tritium source (WGTS), following the design of the Troitsk experiment, and a quench condensed tritium source (QCTS), following the

Mainz design. Alternate measurements with both sources will minimize systematic uncertainties. Both sources will have to be calibrated and controlled extensively. Calibration of the properties of the QCTS will be provided by a series of ^{83m}Kr-conversion line measurements, while the characteristics of the WGTS will be determined by means of an electron gun and of ^{83m}Kr.

Apart from the standard integrating (MAC-E) mode of operation, short-term measurements with the differential time-of-flight (MAC-E-TOF) mode [50] will play an important role in the measuring programme of KATRIN. These additional runs will help to investigate systematic uncertainties – *e.g.* inelastic scattering of the β electrons in the tritium source – with much higher precision than the integral MAC-E-Filter mode would allow.

The detailed spectral information obtained in the MAC-E-TOF mode will also allow to search for non-SM physics like possible small right-handed contributions to the electroweak interactions [54], or tachyonic neutrinos [53]. Also, effects such as the anomaly reported in the Troitsk experiment [43] can be identified and investigated in the non-integrating MAC-E-TOF mode more clearly. Moreover, the resulting distortion in the energy spectrum will stay *local* in a non-integrating spectrometer mode. This in turn will allow to disentangle the effects of non-zero $m(\nu_e)^2$ values from any narrow spectral anomaly close to the endpoint.

The favorable location for a future high precision tritium β decay experiment is the site of Forschungszentrum Karlsruhe (FZK), which offers general infrastructure matching well the extensive experimental demands. In particular, a location on site of FZK offers close proximity to a tritium laboratory (Tritium Labor Karlsruhe, TLK), which is well suited to handle and to process the total tritium inventory of the experiment of about 10^{13} Bq. The hall to house the KATRIN experiment has to be located sufficiently close to the tritium laboratory TLK to allow the continuous supply of tritium gas to the experiment via transfer lines (feed and return tubes). For a linear set-up of all components, as shown in the schematic view of fig. 9, the overall length of the KATRIN hall would be about 70 m. Therefore we propose to set-up and to operate the experiment on the site of FZK.

In the following sections we discuss the experimental parameters relevant for the improvement in statistics and resolution, namely the two tritium sources, the electron transport sections, the two spectrometers and the detector options. This is followed by a discussion of the background and of the systematic uncertainties. Finally, we point out the physics objectives of the KATRIN experiment, in particular we present sensitivity estimates for the electron neutrino mass.

3.2 Experimental parameters

For tritium β decay experiments like KATRIN, which are based on the MAC-E- Filter technique, the ratio of magnetic field strengths in different parts of the experiment (tritium source, magnetic pinch, analyzing plane of the spectrometer and detector) determines several key experimental parameters.

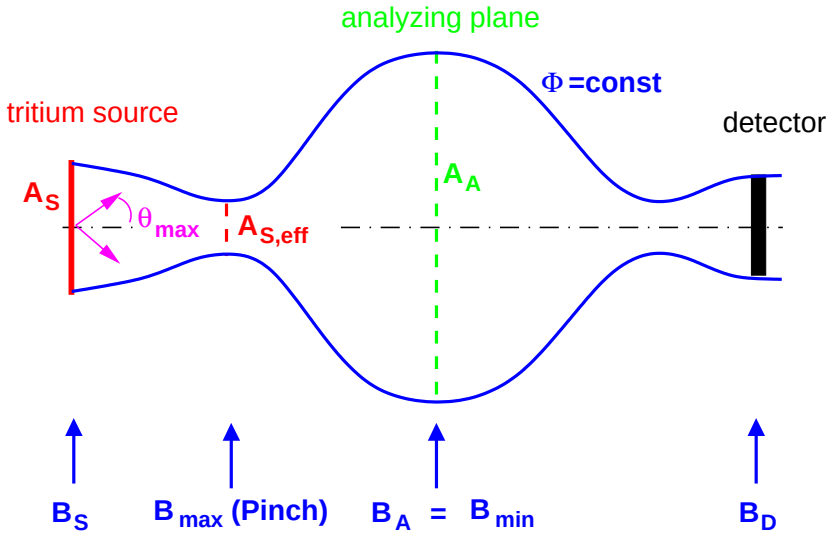

Figure 10: Schematic view of magnetic fields and cross sections (omitting the pre-spectrometer). The magnet field values are $B_{\mathrm{S}} = 6$ T, $B_{\mathrm{max}} = 10$ T, $B_{\mathrm{A}} = B_{\mathrm{min}} = 5 \times 10^{-4}$ T and $B_{\mathrm{D}} = 3$ T (all values are subject to a common scaling factor $f = 0.5 - 1.0$).

3.2.1 Magnetic fields

The geometry and the arrangement of magnetic fields is illustrated schematically in fig. 10. The tritium source with area A_{S} is placed in a magnetic field B_S, which is lower than the maximum magnetic field B_{max} (magnetic pinch). Their ratio determines the maximum accepted starting angle $\theta_{\mathrm{max}} = \arcsin\sqrt{B_{\mathrm{S}}/B_{\mathrm{max}}}$ (see eq. 13). Due to the conservation of the magnetic flux Φ within which the electrons are transported, an effective source area $A_{\mathrm{S,eff}}$ at the magnetic pinch can be defined. The maximum cross section A_{A} of the flux tube is reached in the analyzing plane at the minimum magnetic field B_{A} . The ratio $B_{\mathrm{A}}/B_{\mathrm{max}}$ determines the relative energy resolution according to eq. (12).

The following considerations are based on the assumption of a conserved magnetic flux $\Phi = B_S \cdot A_{\mathrm{S}} = B_{\mathrm{max}} \cdot A_{\mathrm{S,eff}} = B_{\mathrm{A}} \cdot A_{\mathrm{A}}$ of

$$\Phi = f \cdot 5 \cdot 10^{-4}\,\mathrm{T} \cdot \pi(7/2\,\mathrm{m})^2 = f \cdot 192\,\mathrm{Tcm}^2 \tag{14}$$

The common scaling factor f with $0.5 \leq f \leq 1.0$ allows for further adjustments of magnetic fields to their final values. The current values (see fig. 10) have been obtained by optimizing the requirements for adiabaticity, which aims for high magnetic fields. Avoiding the trapping of particles, on the other hand, would favor lower magnetic fields. In addition, technical feasibility and costs were considered.

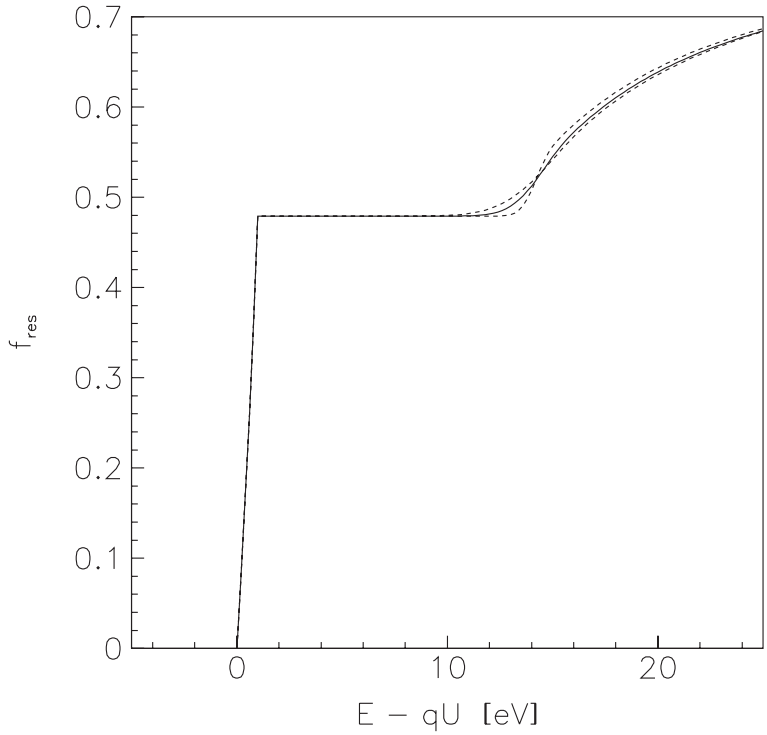

Figure 11: Response function of the KATRIN spectrometer for isotropically emitted electrons with fixed energy E as a function of the retarding energy qU. The energy loss of electrons in the WGTS source (column density $\rho d = 5 \times 10^{17}\,/\,\mathrm{cm}^2$, maximum starting angle $\theta_{max} = 51$ deg) is folded into the response function. To illustrate the uncertainties of the shape of the energy loss function, the experimentally derived function (solid line) and its uncertainties (dashed lines) derived for quench condensed tritium according to reference [46] were used.

3.2.2 Transmission and response function

The transmission function T of a MAC-E-Filter is fully analytical and depends only on the two field ratios $B_\mathrm{A}/B_\mathrm{max}$ and $B_\mathrm{S}/B_\mathrm{A}$:

$$T(E, qU_0) = \begin{cases} 0 & E - qU_0 < 0 \\ \frac{1-\sqrt{1-\frac{E-qU_0}{E}\cdot\frac{B_\mathrm{S}}{B_\mathrm{A}}}}{1-\sqrt{1-\frac{\Delta E}{E}\cdot\frac{B_\mathrm{S}}{B_\mathrm{A}}}} & 0 \leq E - qU_0 \leq \Delta E \\ 1 & E - qU_0 > \Delta E \end{cases} \tag{15}$$

with E denoting the electron energy and qU_0 defining the retarding energy. The total width ΔE of the transmission function from $T = 0$ to $T = 1$ is given by $B_\mathrm{A}/B_\mathrm{max}$ (see 12). The shape of T in this interval is determined by $B_\mathrm{S}/B_\mathrm{A}$, as this ratio defines the maximum accepted electron starting angle θ_max (see eq. 13).

The transmission function T does not take into account the interactions of electrons in the source. Electrons which have undergone inelastic collisions with T_2 molecules in the source have suffered an energy loss and hence have a modified transmission function. These processes can be described by folding of the corresponding

inelastic cross section [46] with the distribution of electron path lengths through the source (including multiple scattering). Folding this energy loss distribution of electrons in the source with the transmission function (15) defines the so-called response function f_{res} of the experiment.

In fig. 11 the response function f_{res} of KATRIN is shown for isotropically emitted monoenergetic particles (with fixed energy E) as a function of the retarding energy qU. The figure is based on the following given standard parameters: a) energy resolution $\Delta E = 1$ eV, b) WGTS column density $\rho d = 5 \cdot 10^{17}/\mathrm{cm}^2$ and c) maximum accepted starting angle $\theta_{\max} = 51°$. The influence of the electric potential drop and the inhomogeneity of the magnetic field in the analyzing plane has not been considered, since these effects can be compensated by a detector with a radial position sensitivity.

Due to the sharpness of ΔE of KATRIN and due to the high threshold of the T_2 excitation, the "no energy loss" fraction of transmitted electrons can clearly be separated from those electrons which have undergone inelastic collisions (see fig. 11). The former fraction corresponds to the sharp rise from 0 to the flat plateau, whereas the latter part represents the second upslope at the abscissa of about 12 eV. The relative amounts of each fraction (*i.e.* the relative height of the elastic plateau in fig. 11) is determined by the column density of the source.

For the case of the continuous β electron spectrum from tritium decay, the f_{res} function of KATRIN implies that the last 10 eV below the endpoint E_0 are fully covered by the elastic plateau of the response function. This means that the region with the highest sensitivity to m_ν is not affected by inelastic processes. Even with a larger measuring interval of 25 eV below E_0, inelastic events contribute to only 2 % of the signal rate (compare fig. 11). Therefore, the systematic uncertainties due to energy losses within the source become dominant only in the analysis of large energy intervals (see fig. 19).

3.2.3 Signal rates

The counting statistics is defined by 3 parameters: the signal rate S, the background rate B and the total measurement time t_{tot}.

For a tritium source of size A_S and column density ρd and maximum starting angle $\theta_{\max}$ accepted by the spectrometer, the signal count rate S very close to the endpoint is proportional to the number of tritium molecules $N(T_2) \propto A_S \cdot \rho d$, the relative accepted forward solid angle $\Delta\Omega/2\pi = 1 - \cos\theta_{\max}$, and the probability of a β electron not to undergo an inelastic scattering process $P_0(\rho d, \theta_{\max})$*:

$$S \propto N(T_2) \cdot \frac{\Delta\Omega}{2\pi} \cdot P_0(\rho d, \theta_{\max}) \tag{16}$$

*Any inelastic scattering process requires a minimum amount of energy loss of 10 eV (s. fig. 11), therefore only the zero loss fraction P_0 contributes to the count rate very close to the endpoint. P_0 is an average over all paths of electrons, starting angles up to $\theta_{\max}$ and starting points within the source column density.

$$= A_{\mathrm{S}} \cdot \rho d \cdot (1 - \cos\theta_{\max}) \cdot P_0(\rho d, \theta_{\max}) \quad (17)$$

$$= \frac{A_{\mathrm{A}} \cdot \Delta E}{E} \cdot \frac{1}{1 + \cos\theta_{\max}} \cdot \rho d \cdot P_0(\rho d, \theta_{\max}) \quad (18)$$

$$= \frac{A_{\mathrm{A}} \cdot \Delta E}{E} \cdot (\rho d)_{\mathrm{eff}} \quad (19)$$

$$\leq \frac{A_{\mathrm{A}} \cdot \Delta E}{E} \cdot \frac{(\rho d)_{\mathrm{free}}}{2} \quad (20)$$

Equation (18) follows through eq. (17) from magnetic flux conservation $B \cdot A = \text{const.}$ and from eq. (12) and (13). Restricting the signal rate to the elastic fraction only is possible due to the narrow energy interval of the KATRIN measurements(as discussed above). Thus the last three terms of eq. (18) can be understood as an effective column density $(\rho d)_{\mathrm{eff}}$ of a virtual source of electrons not undergoing any scattering process and placed in the maximum magnetic field $B_{\max}$ and emitting into the full forward solid angle of 2π from an effective source area $A_{\mathrm{S,eff}} = A_{\mathrm{A}} \Delta E / E$. The signal rate S of eq. (18) increases for all $\theta_{\max}$ with larger column density ρd, but since $P_0(\rho d, \theta_{\max})$ decreases at the same time, the effective column density $(\rho d)_{\mathrm{eff}}$ approaches a maximum asymptotic value (see also fig. 12):

$$(\rho d)_{\mathrm{eff}} = \frac{1}{1 + \cos\theta_{\max}} \cdot \rho d \cdot P_0(\rho d, \theta_{\max}) \overset{d \to \infty}{\to} \frac{(\rho d)_{\mathrm{free}}}{2} = \frac{1}{2 \cdot \sigma} \quad (21)$$

Equation (21) means that averaging over all emitted starting angles and weighting with the accepted solid angle the maximum effective source thickness is restricted to half of the mean free column density $(\rho d)_{free} = 1/\sigma = (2.94 \pm 0.06) \cdot 10^{17}$ cm^{-2}, where σ is the total inelastic cross section at 18.6 keV [46].

Equation (20) shows that the maximum signal rate, which can be achieved is determined by the product of two key experimental parameters: the energy resolution ΔE and the size of the analyzing plane A_{A} of the electrostatic spectrometer. For KATRIN the gain in A_{A} by a factor of about 100 will in parts be counteracted by the improvement of ΔE by a factor 4. On the other hand, the restriction to the elastic fraction will allow to increase the column density substantially with respect to the presently used value of $2.4 \cdot 10^{17}$ molecules/cm^2 [37] without increasing the systematic uncertainties.

3.3 Windowless gaseous tritium source

The windowless gaseous tritium source (WGTS) allows the measurement of the endpoint region of the tritium β decay and consequently the determination of the neutrino mass with a minimum of systematic uncertainties from the tritium source. Such a source was first used at the LANL experiment [33] and developed further and adapted to the MAC-E-Filter by the Troitsk group [39].

Figure 12 can be used to obtain realistic design parameters of the WGTS for KATRIN. The graph shows the ratio of effective to free column density (compare eq.

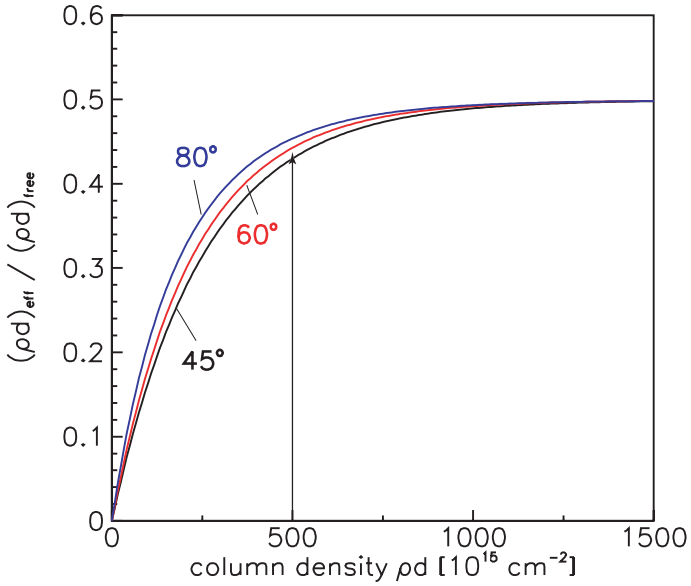

Figure 12: Ratio of effective to free column density $(\rho d)_{\mathrm{eff}}/(\rho d)_{\mathrm{free}}$ (being proportional to the signal rate S) as function of the source column density ρd for different maximum accepted starting angles θ_{max}. The vertical line indicates the proposed WGTS parameters of $\rho d = 5 \cdot 10^{17}$ molecules/cm^2 and $\theta_{\mathrm{max}} = 51°$.

(19), (20)) as a function of the real column density of the source. Choosing the latter as $5 \cdot 10^{17}$ molecules/cm^2 yields a ratio which is reasonably close to the asymptotic maximum for all θ_{max}. With respect to the present Troitsk source the gain in $(\rho d)_{\mathrm{eff}}$ would be a factor of about 1.5. Together with the proposed gain in A_{A} by a factor of 100 and the reduction of ΔE by a factor of 4 the gain factor in signal rate close to the endpoint would be about 40.

The WGTS will consist of a 10 m long cylindrical tube of 70 mm diameter (see fig. 13), filled with molecular tritium gas of high isotopic purity (> 95 %). The tritium gas will be injected by a capillary at the middle of the tube forming there a density of 10^{15} molecules/cm^3. It then diffuses over a length of 5 m to both end faces of the tube, resulting in a linear decrease of tritium density by a factor of 100 from the injection point to the end faces. In order to keep the source strength constant, the tube and the injected tritium gas have to be temperature stabilized to $\pm$ 0.2 degrees. A working temperature around 30 K optimizes the WGTS column density. Then the central T_2 pressure is $4 \cdot 10^{-3}$ mbar. Cooling is achieved by means of circulating He gas of the appropriate temperature in a small pipe thermally coupled to the tritium tube.

It is proposed to place the tritium tube inside a chain of ten superconducting solenoids of 1 m length each. The solenoids will generate a homogeneous magnetic field of $B_S = 6$ T, which adiabatically guides the decay electrons to the end faces (the modular design of the solenoids has been chosen for reasons of quench stability). The ratio of magnetic field strengths at the source and at the pinch magnet $B_{\mathrm{S}}/B_{\mathrm{max}}$

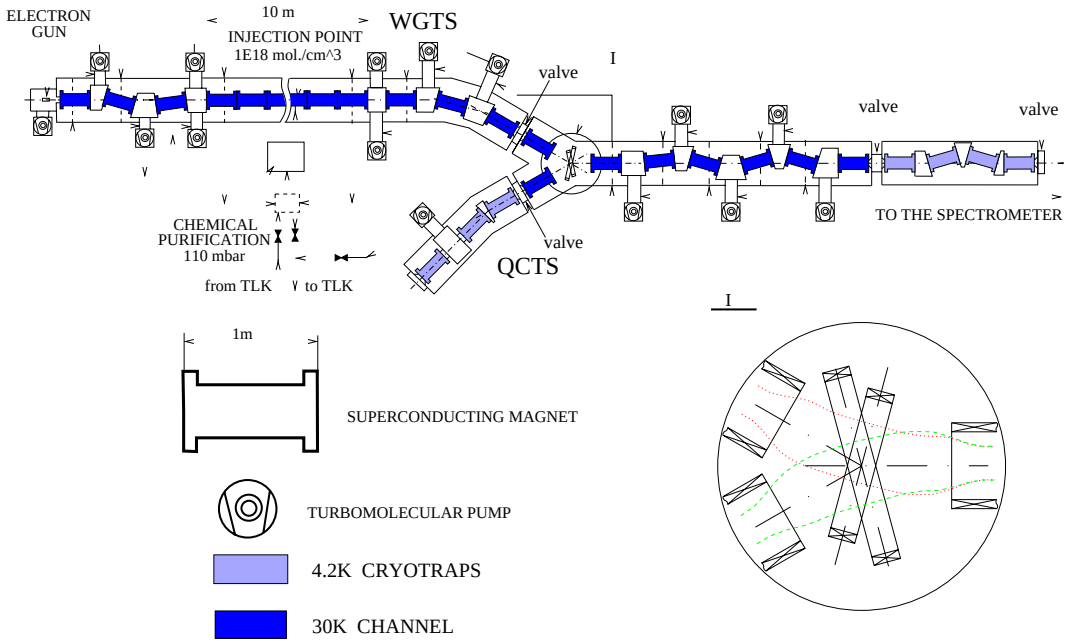

Figure 13: Schematic view of the windowless gaseous tritium source (WGTS) and of the electron transport and differential pumping system. This system includes the y-shaped solenoidal beam switch (also shown enlarged in the inset). Energizing only one of the two short coils and only two of the three transport solenoids allows to select the direction of the electron beam and thus to change the tritium source. The dotted lines in the inset represent the magnetic field lines.

is chosen to be 0.6, so that the maximum accepted starting angle in the WGTS is $\theta_{\max} = 51^\circ$ and the accepted source area is $A_S = 32$ cm^2 (compare eq. (13) and (14)).

The tritium supply for the WGTS will be provided by four double-walled transfer lines from the TLK (one feed and three return lines for different contamination levels). TLK has worked out a procedure to guarantee the supply of tritium with isotopic purity better than 99 % and a negligible content of other gases (^{3}He, ^{4}He). The purity of the supplied tritium will be measured by means of gas chromatography. After processing of the returned gas (detritiation and tritium enrichment) in dedicated glove boxes, the purified tritium will be recirculated to the WGTS.

The main advantages of the WGTS can be summed up as follows:

- investigation of the tritium β-spectrum with the highest possible energy resolution, limited only by the spectrum of final state vibrational and rotational excitations of the daughter molecule $(^3\mathrm{HeT})^+$
- use of a maximum specific activity (high signal rate)
- no perturbing solid state effects (the most serious being self-charging of tritium films [47])
- perfect homogeneity over the source cross section

Attention has to be paid to the following points:

- stability of source strength
- magnetic trapping of charged particles in the local magnetic field minima between the solenoids of the source and the subsequent differential pumping system.

3.4 Quench condensed tritium source

The quench condensed tritium source (QCTS) will run under rather different conditions as compared to the gaseous WGTS source. The design of the QCTS (see fig. 14) largely follows the source concept of the Mainz experiment of a thin film of molecular tritium quench condensed on a graphite substrate.

The QCTS will be mounted on a cold-head of a vertical continuous flow cryostat with 1.6 K base temperature and with total height of 4.5 m. There are three different positions intended for the QCTS source:

- the *measuring position* inside a 5 T split coil magnet of 200 mm diameter and LHe cold bore.
- the *source preparation area* facing a second continuous flow cryostat. This area is equipped with a facility to pre-cool the tritium to 20 K before quench condensing. It contains a laser system for surface treatment (surface cleaning will

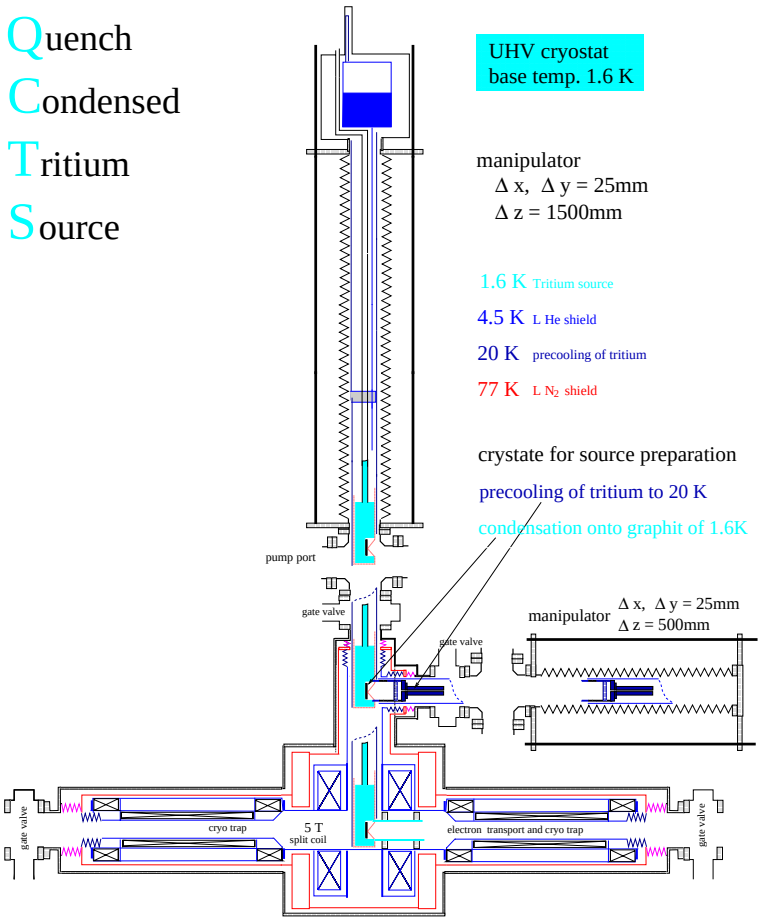

Figure 14: Schematic view of the quench condensed tritium source (QCTS).

be done in-situ by laser ablation) as well as standard diagnostics instruments, like a laser ellipsometer for film thickness measurements.

- the *service position* for maintenance of the QCTS at room temperature.

Figure 14 shows a possible version to connect a vertical cryostat to the horizontal electron beam line by the help of a high field split coil solenoid. Between the QCTS and the y-shape solenoidal beam switch a cryotrapping section is inserted, to avoid condensing of residual gas molecules on top of the condensed tritium film and to reduce the heat load on the QCTS cryostat.

The solid source, which is quench condensed onto a highly oriented pyrolytic graphite crystal, will be working at fixed operating temperature of about 1.6 - 1.8 K. This low temperature is required to suppress surface diffusion and film roughening [41,42]. The thickness and thus also the luminosity of the QCTS will be limited due to self charging [47,60] to a value of about 100 monolayers (1 monolayer is equivalent to a film thickness of about 3.4 Å and corresponds to a column density of the gaseous source of $0.9 \cdot 10^{15}$ molecules/cm^2) [47,48]. The self-charging generates a linear drop of the electric potential from the first to the last film layer of about 20 mV per monolayer. Thus the optimum energy resolution of the main spectrometer for QCTS measurements will be around $\Delta E = 1.6$ eV, which corresponds to a magnetic pinch field of $B_{\max} = f \cdot 6$ T. Due to its lower column density, the QCTS will be run at a higher magnetic field of $B_S = 0.97 \cdot B_{\max}$, resulting in an maximum accepted starting angle of $\theta_{\max} = 80°$ and a source diameter of about 7 cm according to eq. (14). The corresponding gain in source emittance largely compensates the loss in column density. In total the self-charging effect and the reduced energy resolution will limit the *effective* energy resolution of the frozen source to about 2.5 eV. Compared to the present Mainz source with an area of 2 cm^2 and a thickness of 140 ML the new design would correspond to an increase of the count rate by a factor of 30.[†]

The effective lifetime of the new QCTS will be determined by the rate of tritium losses caused by ^{3}HeT$^+$ recoil. This has been found to be of the order of 0.16 monolayer per day [49]. The evaporating tritium is trapped by the LHe cold cryotraps between the QCTS and the beam switch.

As will be discussed later in section 3.11, the QCTS will provide important results with *independent* systematic uncertainties.

3.5 Differential pumping and electron transport system

The electron transport system adiabatically guides β decay electrons from the tritium sources to the spectrometer, while at the same time eliminating any tritium

[†]Both the resolution and the count rate of the QCTS could be improved significantly, if attempts to suppress the self-charging effect turn out to be successful. It is planned to explore this in side experiments in collaboration with Prof. Leiderer in Konstanz. One possibility could be to inject electrons into the source by photo effect at the substrate surface.

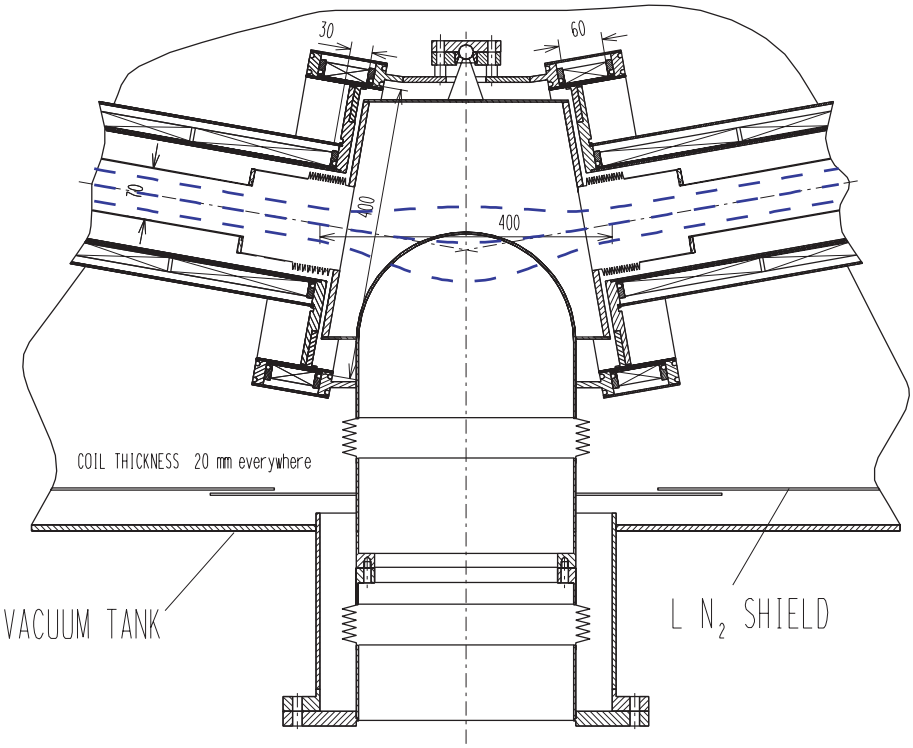

Figure 15: Schematic view of a pumping port between two transport magnets. The central magnetic field line as well the ones describing the envelope of the electron transporting magnetic flux tube (see eq. 14) are illustrated by dashed lines.

flow towards the spectrometer, which has to be kept practically free of tritium for background and safety reasons. The tritium flow (HT molecules) into the spectrometer should be smaller than 10^{-13} mbar l/s $\hat{=}$ $2.7 \cdot 10^6$ molecules/s to limit the increase of background to 10^{-3} counts/s.

The first part of the transport system consists of a differential pumping section directly following the WGTS and consists of 8 transport and pumping stages (see fig. 15). Each transport element consists of a 1 m long tube of 70 mm diameter which is kept at a temperature of 30 K and which is placed inside a superconducting solenoid ($B = 6$ T). The pumping ports are located at the gaps between the transport solenoids, which are tilted by 20° with respect to each other. The field in the port is provided by a pair of split coils. The ports will be equipped with turbo-molecular pumps with a nominal pumping speed of 2000 l/s. The effective pumping speed of the port is estimated to be $s_{\text{eff}} > 700$ l/s. The conductance of the transport tube for T_2 at 30 K is 35 l/s. Hence we estimate an extinction factor of ≥ 20 per stage. The beaming effect due to the long tube changes this result only by 20 % at maximum. The series of 8 differential pumping stages yields an overall tritium extinction factor of $\geq 2 \times 10^{10}$. Assuming that not more than one pump may fail at any time, the extinction factor will still be 10^9. This value is used as the basis for further calculations. The flow out of the T_2 source amounts to 10^{19} molecules/s at each end face and hence less

than 10^{10} molecules/s at the end of the differential pumping chain. In steady state the T_2 gas may be recirculated directly from the pumps to the source many times before the isotopic impurity level reaches the margin of 5 %. Therefore, the T_2 flow from and back to TLK necessary for maintaining the required purity can be kept far below the before mentioned level of 10^{19} molecules/s. The second tritium source of the experiment, the quench condensed QCTS is connected to the electron transport system by a y-shape solenoidal beam switch (see fig. 13).

In the next part of the transport section, the cryotrapping section, all remaining traces of tritium will be trapped onto the liquid helium cold surface of a transport tube surrounded by transport magnets. It will be covered either by a thin layer of charcoal or argon snow for better trapping. Again, 4 individual transport elements of 1 m length and 70 mm diameter are tilted by 20° to each other, thus prohibiting a direct line of sight. The trap will accumulate less than 10^{15} molecules/day which is negligible in view of its huge capacity. Under normal conditions its leakage into the spectrometers should be essentially zero. Safety valves will protect the latter in case of failure, *e.g.* a warmup.

3.6 Electrostatic pre-spectrometer

Between the tritium sources and the main spectrometer a pre-spectrometer of MAC-E-Filter type will be inserted, acting as an energy pre-filter to reject all β electrons except the ones in the region of interest close to the endpoint E_0. For example, working at a retarding energy 100 eV below E_0 , only a fraction of 2×10^{-7} of the total flux of β particles (corresponding to a count rate of the order 1000 s^{-1}) would enter into the main spectrometer. This minimizes the chances of causing background by ionization of residual gas and build up a trapped plasma in the spectrometer. A filter width of $\Delta E \approx 50$ eV would be sufficient for the pre-spectrometer. The flux tube in the analyzing plane would then have a diameter of 1 m, corresponding to a field of 25 mT.

In a second application, the pre-spectrometer will act as a fast switch for running the main spectrometer in the non-integrating MAC-E-TOF mode (see section 3.8).

The pre-spectrometer of KATRIN will have a diameter of 1.2 m and a length of 3.5 m, so that its dimensions are comparable to the existing MAC-E Filters at Mainz and Troitsk. As the designs of the pre- and main spectrometer will be similar, the former will act as a test facility for the larger main spectrometer. Especially important will be the following tests of: a) the technique to achieve an XUHV of below 10^{-11} mbar, b) the concept of using the vacuum vessel itself as main electrode, and c) the electrodynamic concepts to reduce background.

3.7 Main electrostatic spectrometer

A key component of the new experiment will be the large electrostatic spectrometer with a diameter of 7 m and an overall length of about 20 m. This high resolution MAC-

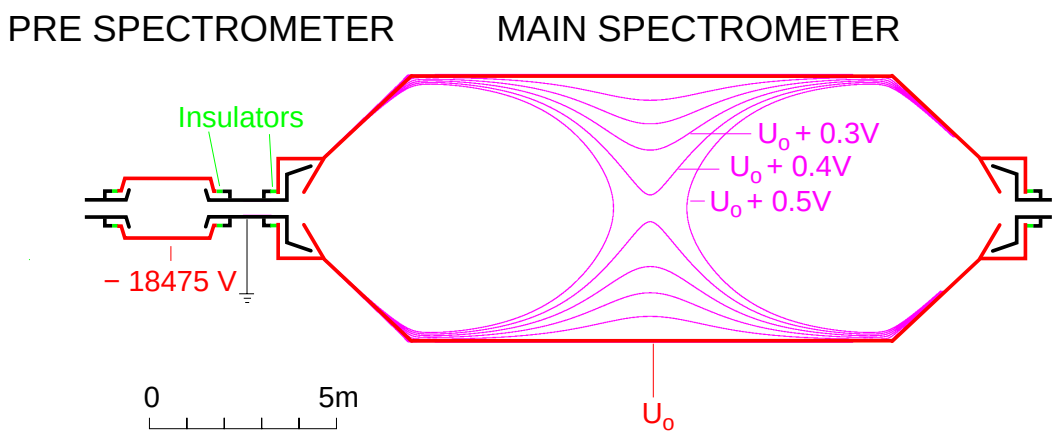

Figure 16: Schematic view of the pre- and main spectrometer. Shown are the electrostatic system and the vacuum vessels (black for ground potential, red for retarding potential and green for insulators), but not the magnets, since the diameter of the tubes at both ends of the spectrometer had to be enlarged in the drawing to become visible. From the equipotential lines with 0.1 V difference (magenta) in the main spectrometer the electrical potential drop in the analyzing plane can be estimated to be 0.45 V.

E-Filter will allow to scan the tritium β decay endpoint with increased luminosity at a resolution of 1 eV, which is a factor of 4 better than present MAC-E Filters.

The current default design is based on the concept that the vacuum tank itself serves as the main electrode of the spectrometer (see fig. 16). This main electrode is connected on both sides by insulators to ground electrodes, which act at the same time as end-caps of the spectrometer vessel. To keep the inner HV system stable and safe, an outer HV shield at a guard potential close to the retarding potential will be installed. Figure 17 shows details of a preliminary design. The advantages of this concept is the minimization of degassing surfaces in the vacuum vessel and the much simplified construction work inside the vessel (as compared to the efforts for mounting and insulating a huge electrode system within the vacuum vessel). In addition, one gains about 10 % of cross section in the analyzing plane.

The actual design of the vacuum vessel as well as the shape and mounting of the ground electrodes is currently being optimized. The present version exhibits a tolerable potential change of about 0.4 V across the analyzing plane. The magnet design provides a homogeneity of the magnetic field in the analyzing plane of better than 10 % . Both kind of inhomogeneities will be compensated by the good spatial resolution of the detector. The electrostatic optimization as well as the corresponding investigation and optimization of the magnetic fields and the simulation of the electron tracks are being pursued further by helps of dedicated 3 dimensional simulation programs.

The combination of large tank dimensions together with the stringent XUHV requirements represents a technological challenge, as XUHV vessels of this size have not been manufactured previously. Therefore, the principal feasibility of the main

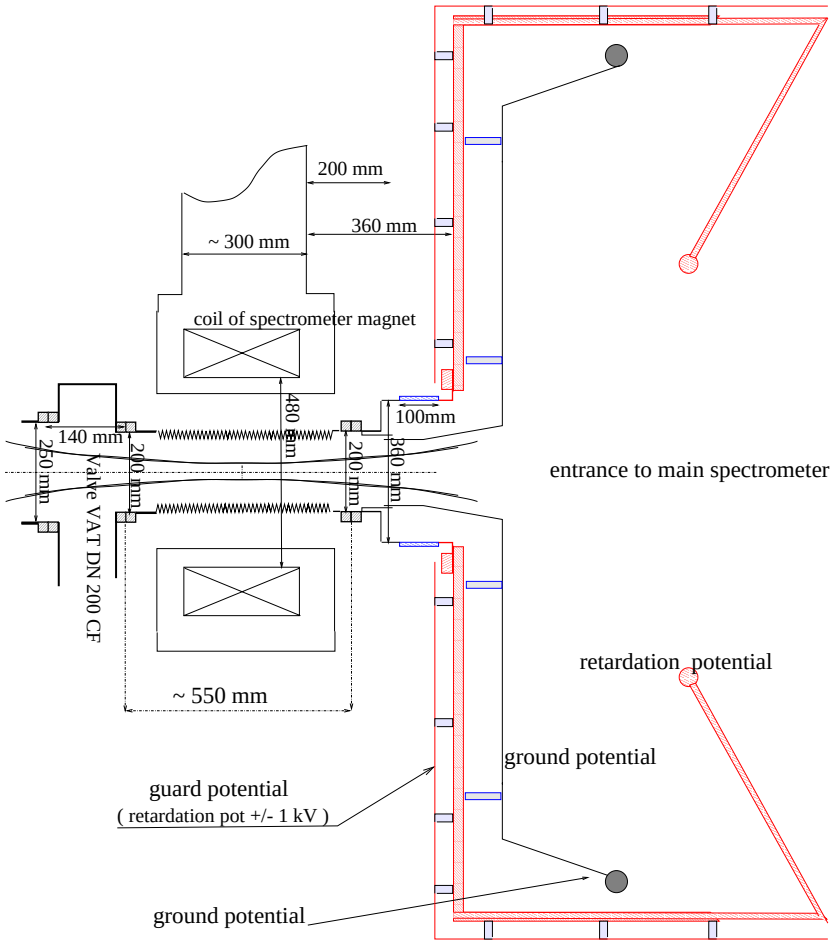

Figure 17: Preliminary design study of the end cap region of the main spectrometer.

spectrometer had to be investigated. A study in collaboration with several industrial partners has demonstrated the feasibility of the construction of a spectrometer of this size and has also yielded a concise construction schedule. During the construction phase special emphasis has to be put on surface preparation techniques. Especially important will be electro-polishing of inner tank surfaces to reduce field emission, and the baking of the vessel at temperatures up to 350° C to reduce the outgassing rate. The latter task will require the installation of a heating system for the spectrometer with 100 kW power. The heat will be transmitted by circulating oil through a tube system around the tank. This solution allows, moreover, to cool down the tank thereafter to a temperature of -20 °C, where outgassing rates are expected to be at least one order of magnitude lower as compared to room temperature. In combination, these techniques will allow to meet the aspired degassing rate from the bulk material (UHV stainless steel) of $< 10^{-13}\,\mathrm{mbar\,l\,s^{-1}\,cm^{-2}}$. The pumping system, which is specified according to this degassing rate, comprises a system of volume getter pumps (2.5 km of SAES getter strips) mounted inside the spectrometer vessel. In addition turbo molecular and ion getter pumps will be installed for pumping non-getterable residual gases (*e.g.* He). Altogether a maximum pumping speed of $s = 5 \cdot 10^5$ l/s will be achieved for getterable gases. This number bears an extra safety margin of an order of magnitude for reaching a final pressure of 10^{-11} mbar[‡]. The early tests with the pre-spectrometer vacuum system based on the same design will allow to optimize the final design.

3.8 Non-integrating MAC-E-TOF Mode

In the recently developed MAC-E-TOF mode [50] one adds on top of the high pass filter of particle energy an equally sharp low pass filter by additional time-of-flight (TOF) measurement through the spectrometer. Both filters together form a narrow band pass. Sufficiently precise TOF measurement is possible even for particles as light as electrons since they are slowed down during their passage through the analyzing potential.

The advantage of the MAC-E-TOF mode is that it provides a non-integrating spectrometer at same energy resolution and similar luminosity as the MAC-E-Filter mode. Ideal applications for such a mode are the investigation of systematic uncertainties like the precise determination of the inelastic scattering cross section in the source. Also the shape of the tritium β spectrum near its endpoint can be investigated with high differential resolution in order to search for new physics (apart from neutrino mass) like tachyonic neutrinos [53] or small right-handed contributions to the electroweak interactions [54], etc.

In tritium β decay the electron start time can only be determined by chopping the flux. Pulsing the retarding potential of the pre-spectrometer to a voltage above E_0 at a

[‡]An alternative concept would be to evaporate a titanium (or equivalent) getter inside the tank. This could provide not only a huge pumping speed but also a homogeneous, well controlled surface potential.

high frequency of about 100 kHz will allow β particles to enter the main spectrometer only within short time windows. The HF pulsing thus enables their time-of-flight analysis. The width of the time windows will reduce somewhat the energy resolution and luminosity. Simulations and experiments at the Mainz setup have shown [50] that in the MAC-E-TOF mode a triangle-like energy resolution function of the same half width as the full width of the transmission function of the integrating MAC-E-Filter can be achieved at a loss of about a factor of 4 in the count rate.

3.9 Detector concept

All β particles passing the retarding potential of the MAC-E-Filter will be guided by a magnetic transport system to the detector. The detector requirements are the following:

- high efficiency for e^- detection and simultaneously low γ background,
- energy resolution of $\Delta E < 600\,\mathrm{eV}$ for 18.6 keV electrons to suppress background events at different energies,
- operation at high magnetic fields,
- position resolution to
  (i) map the source profile,
  (ii) localize the particle track within the spectrometer (for compensation of inhomogeneities of electric potential and magnetic field in the analyzing plane),
  (iii) suppress background originating outside the interesting magnetic flux (*e.g.* coming from the electrodes of the spectrometer),
- for a measurement in a MAC-E-TOF mode, a reasonable time resolution ($\sigma_t < 100\,\mathrm{ns}$),
- for test and calibration measurements ready to take high count rates (up to total rate of order 1 MHz)

The present concept of the detector is based on a large array of silicon drift detectors. The array has to be sensitive over the whole magnetic flux tube, corresponding to a diameter of 11 cm. Silicon drift diodes are significantly advanced in energy and spatial resolution over the rather simple detectors used in the Mainz and Troitsk experiments. The silicon drift detectors will have a very thin dead layer of only 50 nm in order to reduce energy loss and straggling therein and thus to improve the energy resolution. A thin sensitive layer of about 300 μm will help to reduce the γ sensitivity. The small-sized readout electrode – the advantage of silicon drift diodes – reduces electronic noise. An energy resolution of $\Delta E = 600$ eV (FWHM) for 18.6 keV electrons should be achieved.

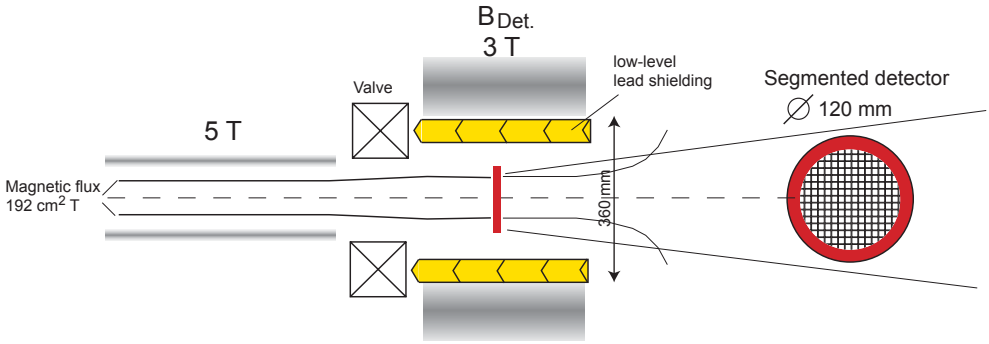

Figure 18: Schematic view of the detector area with magnet configuration and position of the electron detector.

The typical pixel size will be $3 \times 3\,\mathrm{mm}^2$ leading to about 1000 read-out channels allowing a detailed source mapping and reasonably low-sized electronic read-out. Furthermore, as silicon drift diodes are semiconductor based detectors, they can be operated in high magnetic fields of several T. Consequently, the detector will be situated within a special solenoid generating a magnetic field B_D perpendicular to the detector surface. The maximum angle $\theta_{\mathrm{D,max}}$ of incoming electrons at the detector can be limited by the choice of field ratio (see eq. 13) to

$$\theta_{\mathrm{D,max}} \approx \arcsin\left(\sqrt{\frac{B_{\mathrm{D}}}{B_{\mathrm{max}}}}\right)$$

Smaller angles θ reduce backscattering from the detector surface and potential loss of electrons[§].

The detector will be surrounded by low-level passive shielding and an active veto counter to reduce background. Figure 18 shows a view of the schematic setup of the solenoids as well as the position of the detector surface.

For a later stage of the experiment a segmented bolometer is considered as detector. This type of detector has the advantage of a superior energy resolution (as compared to Si-detectors). For cryogenic detectors, resolution values of *e.g.* $\sigma_E \approx 5\,\mathrm{eV}$ at 60 mK for short term measurements of X-rays of 6 keV have been reported [52)]. In high magnetic fields the detector performance was even improved. A better energy resolution of the detector will play an important role, if the relevant sources of background -in particular those from the spectrometer itself (see the following section 3.10)- have an energy distribution, which is sufficiently wider as (or separated from) the energy interval close to the endpoint. In this context it is important to note that recent data from the Mainz experiment show that -within the statistical precision of about 25 eV- the mean of the background line originating from the spectrometer

[§]Although most of the backscattered electrons will be magnetically or electrostatically reflected back onto the detector, the two additional passages through the dead layer will shift a part of the electron signal out of the predefined energy window.

coincides with the filter potential. However, the limited energy resolution of the detector at Mainz of $\Delta E = 1.4$ keV (FWHM) does not allow the detection of a possible fine structure of the energy distribution of the background events.

A cryogenic bolometer would need a proper 4π heat shield at LHe temperature. This would require another cold chicane for the electron transport to the detector to prevent a direct line of sight into the warm spectrometer. A significant amount of R&D work will be necessary to reach the energy resolution aimed at for a whole array of medium size detectors.

More detailed studies are under way to define a final detector design and setup as well as more quantified detector requirements. However, arrays of Si drift diodes and bolometers represent two promising concepts for the detection of low energy electrons in KATRIN.

3.10 Background

The experiments at Mainz and Troitsk observe nearly the same count rate of background events of about 10 mHz from their spectrometers, although the volume of the Troitsk spectrometer is 2 times larger and the residual gas pressure is 10 times higher. This is not a contradiction to the principle of a strong dependence of the background rate on the residual gas pressure in the spectrometer, seen both at Mainz and Troitsk. It shows, however, that the background rate also depends on other critical parameters, such as *e.g.* the shape and strength of the electric and magnetic fields. This fact and the detailed background investigations at Mainz and Troitsk under different conditions make us confident, that we will be able to reach about the same level of background rate of 10 mHz also with the large KATRIN spectrometer.

To allow a more detailed discussion, the different sources of background are described in the following:

- Environmental radioactivity and cosmic rays around the detector
  This background source can be reduced by using selected materials, by active and passive shielding and by a detector with good intrinsic energy resolution. At Mainz this background contributes with a rate of about 1 mHz. The same level can be obtained with the KATRIN detector. Although it will be 20 times larger in area, the background rate can be reduced by the same factor by the at least 2 times better energy resolution, an about 2 times thinner active layer and a 5 times better shielding.

- Tritium decays in the main spectrometer
  In about 15 % of all β decays of molecular tritium the remaining $^3HeT^+$ daughter ion gets further ionized and a low energy shake off electron accompanies the β electron. If the β decay takes place in the detector-facing half of the spectrometer, the electron will be accelerated and collimated onto the detector. There it will be detected with an energy close to that of the retarding energy

qU_0, which fills most of the spectrometer volume. Therefore it can not be distinguished from the signal electrons with present detectors. The only way to avoid this kind of background is a very stringent limit on the tritium partial pressure inside the main spectrometer. A T_2 partial pressure of $p(T_2) \simeq 10^{-20}$ mbar causes a background rate of 1 mHz, which is the maximum tolerable one from this source. The differential pumping and cryotrapping sections as well as the large pumping speed in pre and main spectrometer will guarantee this low T_2 partial pressure.

The β particles from T_2 decay within the spectrometer volume can contribute even stronger to this indistinguishable background by secondary reactions. Born at high starting angle in the low field B_A , they will be trapped in this magnetic bottle and cause ionizations of the residual gas [37]. However, this background can be suppressed by obeying XUHV conditions such that the chance of ionization is low within the storage time. The latter is limited by synchrotron radiation [40] and can be further shortened by breaking the cylindrical symmetry of the fields.

- Cosmic rays
  Cosmic rays can create secondary charged particles like δ-electrons, which then emerge from the electrodes and penetrate into the spectrometer, where they are guided by the magnetic field. Low energy charged particles will stay always close to the outer walls of the spectrometer and can not reach the central magnetic flux, which is collimated onto the detector. These secondary charged particles therefore cannot contribute directly to the background. But they can create ions with much larger cyclotron orbits crossing the magnetic flux tube. Accelerated further by the electric field, these ions then have the chance of producing slow electrons by various tertiary reactions with the residual gas like ionization, charge exchange to negative ions with subsequent electron detachment etc. H^- ions have eventually been observed at the detector. A chance to undergo such tertiary reactions under UHV conditions exists only for trapped particles, however.
  Measurements with the Troitsk and Mainz setup using an external γ-ray source to create δ-electrons resulted in a suppression factor of background electrons with respect to the primary produced δ-electrons of about 10^{-6}. The much larger dimensions and the much better vacuum of the KATRIN main spectrometer will improve this suppression factor and compensate the factor from the increased inner surface. Test experiments with the pre-spectrometer in 2002 will check whether cosmic rays are indeed of minor concern for the background.

- Trapped particles
  Measurements with the existing MAC-E-Filters have shown that the background rate can change abruptly, following time constants of minutes to hours and showing hysteresis like effects. This behavior must be due to trapped par-

ticles inside the spectrometer and chain reactions may sustain a plasma (like in a penning gauge) and release electrons to the detector. In principle, MAC-E-Filters can have phase space regions in which particles of either charge can be trapped, particularly in case of an awkward field design. The hypothesis that traps contribute to the background is further supported by the fact that at Mainz "heating" of the trapped particles by a high frequency electric AC field decreases and stabilizes the background count rate.

Although the KATRIN spectrometer has a much larger volume than the present spectrometers, the increase of dimensions and the careful electrostatic and magnetic design will also allow to reduce the electric fields and field emission from surfaces. Furthermore the design will improve the magnetic shielding of the central magnetic flux from charged particles originating at the electrodes or walls. In addition, new concepts of active background suppression will be tested. To avoid the trapping of charged particles in regions corresponding to magnetic bottles and the resulting chain of ionization processes, the axial field symmetry may be broken by bending of the magnetic flux tube. Alternatively, electric dipole fields may be applied. The resulting transverse $\vec{R} \times \vec{B}$ drift (with $\vec{R}$ defining the radial vector) in a non-straight geometry or $\vec{E} \times \vec{B}$ drift in the case of an electric field perpendicular to the magnetic field lines should remove stored particles from the sensitive flux tube on time scales of less than 1 s. Such investigations are foreseen at the present spectrometers as well as at the pre-spectrometer. In parallel, ray tracing of particles on the computer will minimize trapping possibilities by optimized field design and improve our understanding of these processes.

3.11 Systematic uncertainties

For a high sensitivity tritium β experiment like KATRIN, the interesting region of the β spectrum close to the endpoint E_0 is very narrow. A narrow energy interval means that the count rate statistics will be limited, i.e. that the statistical error is rather large. On the other hand, a narrow energy interval strongly reduces systematic errors. The systematic uncertainties of the current tritium β experiments mainly arise from processes connected to atomic and molecular physics, such as inelastic scattering of tritium β electrons in the tritium source. This process as well as various other sources of systematic uncertainties are discussed in more detail below.

- Inelastic scattering
  The inelastic scattering of electrons in the tritium source is one of the dominant sources of the systematic background. The cross section of this process [46)] has a rather high threshold of more than 12 eV (see fig. 11). Thus, the last 12 eV of the β spectrum, which carry the main information on the ν mass, are free of any inelastic scattering events. This holds also strictly for the measured spectrum,

because the transmission function of a MAC-E-Filter has no high energy tail (see fig. 11) due to energy conservation.

Confining the measurements to the elastic fraction, much thicker tritium sources can be used. The present relative uncertainties of the total cross section are 2 % for gaseous tritium and 5 % for quench condensed tritium sources [46]. The shape of the energy loss function is well measured for gaseous tritium and reasonably well known for quench condensed tritium as illustrated in fig. 11. Still the knowledge of both the total as well as the differential cross section can be improved further by dedicated measurements with quasi-monoenergetic electron sources (electron gun or K-32 conversion from ^{83m}Kr) using the MAC-E-TOF mode of the new KATRIN spectrometer. Residual systematic uncertainties will be reduced accordingly.

- Column density and homogeneity of the tritium source
  The column density of the WGTS and the QCTS is measured and monitored in two ways:
  (i) The tritium count rate determined with the detector gives online a spatially resolved tritium column density measurement in combination with online mass spectrometry. For this purpose a particular measurement point further below the tritium endpoint with enhanced count rate will be chosen.
  (ii) Offline measurements with the electron gun will control the column density of the WGTS from the ratio of the inelastic to elastic fraction, whereas that of the QCTS is determined by ellipsometry. A precision of 1 % in units of the mean free column density $(\rho d)_{\mathrm{free}}$ can be achieved safely.

- Backscattering
  The coefficient describing the fraction of electrons backscattered from the graphite substrate of the Mainz experiment is $3 \cdot 10^{-5}$/eV and even smaller for the Troitsk setup. Therefore, backscattering does not play any significant role for the narrow energy interval below the β endpoint considered for the KATRIN experiment.

- Final states
  The first electronic excited state of the ^{3}HeT$^+$ daughter molecule has an excitation energy of 27 eV [56]. Therefore excited states do not play any role for the energy interval considered for the KATRIN experiment, only the decay to the ground state of the $(^3\mathrm{HeT})^+$ daughter molecule, which is populated with 57 % probability, has to be taken into account. Due to the nuclear recoil, however, a large number of rotational-vibrational states with a mean excitation energy of 1.7 eV and a width of 0.4 eV is populated. This distribution follows the Franck-Condon principle; its precision depends on the knowledge of the ground state wave function, which is extremely good [57]. Therefore, no significant uncertainty arises from the rotational-vibrational excitation of the final ground

state. Also a contamination of the T_2 molecules by HT does not matter in first order: The shift of the mean rotational-vibrational excitation of HT with respect to T_2 is compensated by a corresponding change of the nuclear recoil energy of HT with respect to the 1.5 times heavier T_2 molecule [56]. However, this distribution ultimately limits the resolution which can be obtained in T_2 β decay .

- Transmission function
  Since the transmission function (eq. 15) depends only on the relative field values and potentials, it is insensitive to mechanical adjustment. The inhomogeneity of the magnetic field and the electric potential can be calculated precisely. In addition, the shape of the transmission function will be checked by a point-like test source of K-32 conversion electrons from ^{83m}Kr or by an electron gun, which is moved across the magnetic flux tube at the position of the QCTS.
  Fluctuations of the absolute position of the transmission function are more critical. A simple relation connects an additional unknown Gaussian broadening of width σ_g (*e.g.*- caused by fluctuations of the absolute value of the retardation potential qU_0) to a shift of m_ν^2 [58]:

$$\Delta m_\nu^2 = -2 \cdot \sigma_g^2 \tag{22}$$

  Therefore, the noise and the stability of the high voltage has to be below 70 mV to limit its contribution to Δm_ν^2 to a maximum value of 0.01 eV^2.

- Trapped electrons in the WGTS
  Each β electron which is trapped in a local magnetic minimum due to eq. (13) will suffer inelastic scattering events. Rarely these processes are accompanied by a momentum transfer large enough to scatter the electrons into the cone of polar angles small enough to leave the trap. Before being freed finally, they hence accumulate an energy loss being larger, most probably, than the energy region of interest below the endpoint. Furthermore the magnets will be designed to avoid large trapping volumes in the WGTS. Magnetic traps cannot be avoided in the region of differential pumping ports (see fig. 15). In the bent, however, the electrons will be driven out of the trap by synchrotron radiation. Moreover, the T_2 density and hence the decay rate is dropping very fast along the differential pumping chain.

- Solid state effects for the QCTS
  Several additional systematic uncertainties are connected with the QCTS:

  - Neighbor excitation
    The sudden change of nuclear charge in β decay can excite even neighboring T_2 molecules. According to ref. [59] the probability is 5.9 % in a closely packed single crystal and the mean excitation energy is given as 14.6 eV, based on the spectrum of free hydrogen molecules. For the analysis of the

Mainz data the former number has been lowered to 4.6 % and the latter raised to 16.1 eV [38]. The changes account for the reduced density of the quench condensed film [38] and for the observed shift of the energy loss spectrum of 18 keV electrons passing gaseous and solid hydrogen, respectively [46]. This shift is also corroborated by quantum-chemical calculations [62]. To be conservative the changes are taken fully into account as systematic uncertainties [38]. To improve on this situation a quantum chemical calculation of the neighbor excitation for the quench condensed T_2 case would be useful. For the KATRIN data this effect will play a marginal role, since inelastic events will do not contribute to the signal in a significant way.

- Self-charging
  Due to the continuous radiation of β particles a quench condensed T_2 film – being an excellent insulator – charges up. This effect has been studied in detail and explained by a satisfactory model [47,60]. In the temporal equilibrium self-charging generates a linear drop of the electric potential across the T_2 film of about 20 mV per monolayer. For the Mainz analysis [49] 20 % of the total self-charging effect was taken into account as systematic uncertainty. Refined measurements could probably reduce this uncertainty by another factor of 2. More serious than systematic uncertainties is the 2 eV broadening of the spectrum due to self-charging of the QCTS since it reduces the sensitivity on m_ν (see below).
- Longterm behavior
  A tritium loss of about 0.16 monolayer per day was observed at the Mainz QCTS. The effect is due to sputtering of T_2 molecules by nuclei recoiling from β decays. It cannot be avoided but has been monitored precisely by measuring the longterm decrease of the count rate. In parallel a condensation of H_2 from the residual gas was observed by ellipsometry at the end of the run. This effect will be avoided in the KATRIN experiment by providing more effective cryogenic vacuum conditions at the QCTS.

In summary, the main systematic uncertainties arise from the inelastic scattering and the degree of stability of the retarding voltage. For the case of the QCTS source the uncertainties of the solid states effects have to be added. At KATRIN the systematic uncertainties will be substantially reduced by

- the much smaller energy interval of interest below the endpoint E_0,
- additional control measurements at ultrahigh resolution in both the MAC-E- and MAC-E-TOF mode,
- the better stability of the high voltage,
- the higher T_2 concentration and

- the improved vacuum conditions

with respect to the present experiments. As will be shown in section 3.13, this improvement will allow KATRIN to reach the goal of a sub-eV sensitivity on the neutrino mass.

3.12 High voltage stability and energy calibration

As pointed out in section 3.11, a high voltage stability of better than 70 mV is needed. This requirement corresponds to a precision of a few ppm, which is state of the art for a system consisting of a high voltage (HV) power supply, a HV divider and a digital voltmeter. The longterm stability of this system will be checked repeatedly by measuring the K-32 conversion line of ^{83m}Kr, which has an energy of about 17.825 keV and a width of 2.83 eV (FWHM) [61]. Such a measurement can be performed by quench condensing krypton onto the graphite substrate of the QCTS. For the WGTS this would require a 100 times larger amount of krypton circulating in the closed pumping cycle. Also the temperature has to be raised from 30 K to about 70 K to avoid condensation of krypton. One can also consider to use a third independent electrostatic spectrometer, like the Mainz MAC-E-Filter, for monitoring of the high voltage by measuring the K-32 conversion line continuously. Since the half life of ^{83m}Kr is 1.83 hours only, one would install the mother ^{83}Rb (half life: 86 days) as a source, continuously producing ^{83m}Kr in situ. First investigations of this technique look promising [63] but chemical and solid state effects on the conversion line position have to be thoroughly examined. Since the HV dividers and digital voltmeters are generally more stable than the HV power supplies themselves, the quality of the β spectrum accumulated during long measuring times can be improved by the method [64].

Besides stability a precise, absolute calibration of the spectrometer voltage would be very valuable as an important check, since the endpoint energy E_0, derived from the measured β spectrum, could be compared to the independently measured mass difference $\Delta M(^3\mathrm{He}, \mathrm{T})$, which is known from measurements with absolute precision of 1.7 eV [65]. This measurement from the early nineties could be improved by about one order of magnitude using state of the art equipment [66]. Then the comparison at a 0.1 eV level of the experimental endpoint energy E_0 with the external mass difference $\Delta M(^3\mathrm{He}, \mathrm{T})$ will check for unknown systematics of the KATRIN experiment. The option to use the external mass difference $\Delta M(^3\mathrm{He}, \mathrm{T})$ directly as fixed input parameter in the analysis of the β spectrum to improve its sensitivity on m_ν will be discussed in section 3.13.

3.13 Sensitivity on the electron neutrino mass

For the calculation of the expected sensitivity on the electron neutrino mass we restrict the discussion to simulated data from the WGTS. As shown in section 3.2, the signal

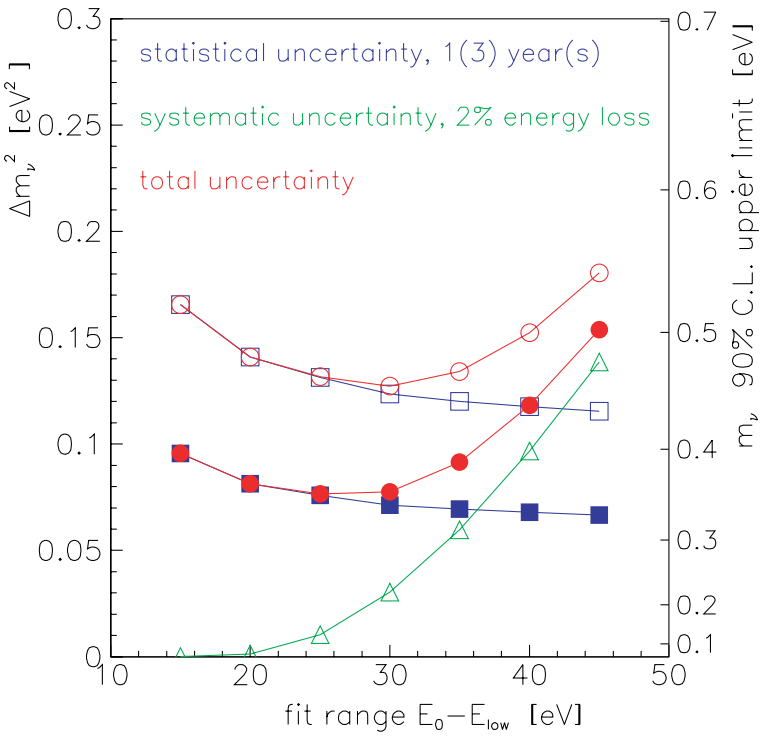

Figure 19: Estimates of the sensitivity on the electron neutrino mass for a specific set of parameters (see text for details) shown as a function of the fit range of the electron spectrum below the endpoint E_0. The left axis denotes the 1σ error of m_ν^2, the right axis denotes the 1.64σ or 90% confidence upper limit on the absolute electron neutrino mass under the assumption of zero mass. Squares describe statistical uncertainties after 1 and 3 years (open and filled squares, respectively), triangles show the systematic uncertainty and circles represent the total uncertainty.

rate S of electrons near the endpoint E_0 (see eq. (16)–(20)) can be expressed in terms of the energy resolution $\Delta E/E$, the column density ρd and the maximum accepted starting angle $\theta_{\max}$. Apart from the count rate or signal strength near the endpoint, sensitive parameters of the neutrino mass evaluation are the background rate b, the actual interval below E_0 used for measuring and fitting the spectrum, as well as systematic uncertainties discussed in sec. 3.11. As pointed out there, the dominant systematic uncertainty using the WGTS is inelastic scattering. In our discussion we consider this uncertainty as the only one. We used the present uncertainties, characteristic for the Troitsk experiment [46], although an improvement by a factor of two at KATRIN can be expected.

Fig. 19 shows the results of simulations based on a realistic parameter set: energy resolution $\Delta E = 1\,\mathrm{eV}$, source surface area $A_S = 29\,\mathrm{cm}^2$, column density $\rho d = 5 \cdot 10^{17}/\mathrm{cm}^2$, maximum accepted angle $\theta_{\max} = 51°$ for β electrons starting from the source, and total background rate of 11 mHz. For small fit ranges near the endpoint, the sensitivity is limited by statistics whereas for larger intervals systematic uncertainties become dominant. After one (three) year(s) of measuring time, the 1σ error on the observable Δm_ν^2 is expected to be smaller than $0.14\,\mathrm{eV}^2$ ($0.08\,\mathrm{eV}^2$), as can be

seen from the left ordinate in fig. 19. Having simulated the spectra with zero neutrino mass, the one year measurement leads to an upper limit of the mass itself of 0.5 eV at 90% confidence. This upper limit L(90%) is connected to the error on Δm_ν^2 via $L(90\%) = \sqrt{1.64 \cdot \Delta m_\nu^2}$. After three years of measuring time, this limit will improve to

$$m(\nu_e) < 0.35\ eV \qquad \text{at } 90\,\% \text{ confidence,}$$

if no finite neutrino mass is observed. This sensitivity improves the existing limits by almost one order of magnitude and also demonstrates the discovery potential of KATRIN for an electron neutrino mass in the sub-eV range.

The sensitivity estimates given above are based on the assumption that KATRIN reaches the same background level as the present Mainz and Troitsk experiments. As pointed out in section 3.10 this assumption is reasonable. Significantly larger or smaller rates of background would not change the sensitivity of KATRIN to $m(\nu_e)$ very much. If the background rate would be 5 times higher, the limit on $m(\nu_e)$ would be worse by a factor 1.4, if the background would be 5 times lower, the limit on $m(\nu_e)$ would improve by a factor 1.2 .

The sensitivity which can be obtained by measurements with the QCTS, assuming the uncertainties of the Mainz experiment, will be 2 times worse than the WGTS sensitivity. The main disadvantage is the self-charging, which will limit the signal rate S as well as the energy resolution ΔE as pointed out in section 3.4. If the self-charging effect cannot be overcome, the QCTS will still provide checks with well understood and complementary systematic uncertainties and as a backup source, moreover.

In the standard fit procedure the four free parameters are m_ν^2 , E_0, amplitude A and background rate b. As mentioned in section 3.12, the endpoint energy E_0 can be obtained from an independent measurement of the ^{3}He-T mass difference $\Delta M(^3\mathrm{He}, \mathrm{T})$. Does it make sense to put this number into the analysis as external fixed input parameter for E_0, in order to decrease the number of highly correlated fit parameters by one? The correlation of m_ν to E_0 in the fit increases linearly with increasing the distance to the endpoint[67)], which is the neutrino energy. Therefore we have to restrict ourselves to measure only a very small interval below E_0 of the last 5 eV. Taking into account the width of the transmission function ΔE and the average rotational vibrational excitation of the ground state of 1.7 eV the effective endpoint is about 2.2 eV lower, thus the interval quoted corresponds essentially to about the last 3 eV of the spectrum. Fixing the endpoint energy the statistical uncertainty of m_ν^2 for a 3 years measurement under standard conditions (see above) becomes Δm_ν^2 = 0.05 eV^2 . The main systematic uncertainty will come from the external endpoint energy, which results for this situation in Δm_ν^2 /$\Delta E_0 \approx 2$ eV. *E.g.* an uncertainty of $\Delta E_0 = 20$ meV corresponds to an systematic uncertainty of 0.04 eV^2 . Thus, if a 1 ppm precision in the ^{3}He-T mass difference $\Delta M(^3\mathrm{He}, \mathrm{T})$ and the absolute calibration of KATRIN could be achieved the sensitivity on m_ν could be improved further by using an external $\Delta M(^3\mathrm{He}, \mathrm{T})$ value in the analysis.

4 Outlook and Conclusion

Outlook

We have demonstrated the feasibility of a tritium β decay experiment with sub-eV sensitivity. The realization of the proposed KATRIN experiment will, nevertheless, be a technological challenge, especially with regard to the extreme UHV requirements of the large electrostatic spectrometer vessel. In this context, the existing infrastructure and technical expertise of Forschungszentrum Karlsruhe will make it the favorable location for the experiment. The overall costs of the experiment are estimated to be about 17 million Euros (salaries not included), with the main costs arising from the spectrometer vessel (3.5 M Euros estimated) and the solenoid system (6.7 M Euros estimated).

Following the first presentation of the KATRIN project at an international workshop at Bad Liebenzell [69], the KATRIN Collaboration was formally founded in June 2001. The future time schedule of the KATRIN project calls for a full proposal to be submitted in early 2002, followed by requests to the funding agencies later that year. While systematic studies of background processes have already been performed at Troitsk and Mainz, further detailed studies as well as prototyping experiments and further design optimizations will be carried out over the next months. On condition that the funding requests will be approved, the construction works for KATRIN could be finished by the end of 2005. The commissioning and first test measurements of KATRIN could then start in 2006, with long term data taking starting later that year. We aim for a strong collaboration to build and perform the proposed experiment and would welcome new participants.

Conclusion

In this paper we have discussed the physics and technique of a next generation tritium β decay experiment, which would have an unprecedented sensitivity to the electron neutrino mass. The experiment we propose has the potential to improve the sensitivities of the present experiments in Troitsk and Mainz by *one order of magnitude*. With an estimated sensitivity of $m(\nu_e) = 0.35$ eV , KATRIN could investigate for the first time the sub-eV neutrino mass range by a direct kinematic measurement.

Neutrino masses are of special interest for cosmology and astrophysics, as the relic neutrinos left over from the Big Bang could play a significant role as neutrino hot dark matter in the evolution of large scale structures in the universe. If the electron neutrino mass falls into the sensitivity range of KATRIN, the role of relic neutrinos in structure formation could be fixed (taking into account the recent results of neutrino oscillation experiments). If, on the other hand, the ν_e-mass will not be in the range of the sensitivity, the constraint on the contribution Ω_ν of relic neutrinos to the total matter-energy density of the universe could be improved by one order of magnitude, thereby limiting the cosmological significance of neutrinos. Therefore,

one of the main motivations of KATRIN is to measure or to constrain the parameter Ω_ν. In this context, the results of KATRIN would be an important input parameter for cosmological studies, especially for the analysis of future high precision, satellite based cosmic microwave background measurements (MAP and Planck).

Apart from astrophysics and cosmology, the absolute mass scale of neutrinos plays a central role for particle physics. As the Standard Models of particle physics offers no explanation for fermion masses and mixing, the determination of the ν-mass scale will be of fundamental importance for extended theories beyond the Standard Model dealing with the mechanisms of mass generation. As ν masses are much smaller than the masses of the other fermions, it will most probably be the neutrino mass scale which will set the scale for new physics.

The only method to investigate the absolute mass scale of neutrinos in a *model independent* way is the high precision spectroscopy of β decays. For this class of experiments, only tritium β decay experiments using electrostatic spectrometers will allow to reach the sub-eV mass range in the nearer future. The experiment we propose will push this technique to its technological limits, especially with regard to the dimensions of the electrostatic spectrometer and the source strength of the gaseous molecular tritium source. Thus, according to our present knowledge, KATRIN represents an 'ultimate' tritium β decay experiment.

The proposed next-generation tritium β decay experiment will be complementary to the numerous future oscillation experiments using solar, atmospheric and accelerator neutrinos. These experiments will determine with great precision the neutrino mixing parameters as well as the mass splittings among the different neutrino mass eigenstates, but will not yield information on the absolute values of neutrino masses. KATRIN will also be complementary to future $0\nu\beta\beta$ experiments, which will provide important information on Majorana neutrino masses. It is only the combination of the different results from neutrino oscillation experiments, $0\nu\beta\beta$ experiments and tritium β decay experiments which will allow us to get the 'full picture' of neutrinos.

5 References

1) Y. Fukuda *et al.*, Phys. Rev. Lett. **81** (1998) 1562,
   Y. Fukuda *et al.*, Phys. Rev. Lett. **85** (2000) 3999
2) S. Fukuda *et al.*, Phys. Rev. Lett. **86** (2001) 5656
3) Q.R. Ahmad *et al.*, Phys. Rev. Lett. **81** (2001) 071301
4) R. Barbieri *et al.*, Phys. Lett. **B90** (1980) 91,
   T. Yanagida, Prog. Theor. Phys. **64** (1980) 1103,
   R.N. Mohapatra *et al.*, Phys. Rev. Lett. **44** (1980) 912
5) A. Zee, Phys. Lett. **B93** (1980) 389,
   L. Wolfenstein, Nucl. Phys. **B175** (1980) 93,
   D. Chang, A. Zee, Phys. Rev. **D61** (2000) 071303
6) Y. Farzan, O.L.G. Peres, A. Yu. Smirnov, `hep-ph/0105105`

7) S.M. Bilenky, S. Pascoli, S.T. Petcov, hep-ph/0104218
8) H. Georgi, S.L. Glashow, Phys. Rev. **D61** (2000) 097301,
V. Barger *et al.*, Phys. Lett. **B437** (1998) 107,
J.A. Casas *et al.*, Nucl. Phys. **B569** (2000) 82
9) M. Kamionkowski *et al.*, Ann. Rev. Nucl. Part. Sci. **49** (1999) 77
10) G. Fuller, Phys. Rev. **D61** (2000) 123005
11) D.E. Groom *et al.*(Particle Data Group), Eur. Phys. J. **C15** (2000) 1
12) M. Tegmark *et al.*, Phys. Rev. **D63** (2001) 043007
13) MAP experiment: http://map.gsfc.nasa.gov/
14) PLANCK experiment: http://astro.estec.esa.nl/SA-general/Projects/Planck/
15) F.v. Feilitzsch , Proc. of the Int. Conf. Neutrino 2000, Sudbury, Canada,
Nucl. Phys. **B** (Proc. Suppl.) **91** (2001), 66
16) A. Suzuki *et al.*, Nucl. Phys. **B77** (Proc. Suppl.) (1999) 171
17) K. Nakamura *et al.*, Nucl. Phys. **A663-664** (2000) 795c
18) Minos Collaboration, NuMI-L-63 MINOS proposal (1995)
19) A. Bazarko *et al.*, Proc. of the Int. Conf. Neutrino 2000, Sudbury, Canada,
Nucl. Phys. **B** (Proc. Suppl.) **91** (2001), 210
20) H.V. Klapdor-Kleingrothaus *et al.*, hep-ph/0103062
21) E. Fiorini, Proc. of the Int. Conf. Neutrino 2000, Sudbury, Canada, Nucl.
Phys. **B** (Proc. Suppl.) **91** (2000) 262
22) G.B. Mills *et al.*, Proc. of the Int. Conf. Neutrino 2000, Sudbury, Canada,
Nucl. Phys. **B** (Proc. Suppl.) **91** (2001), 198
23) K. Eitel *et al.*, Proc. of the Int. Conf. Neutrino 2000, Sudbury, Canada, Nucl.
Phys. **B** (Proc. Suppl.) **91** (2001), 191
24) T.J. Loredo and D.Q. Lamb, ANYAS **571** (1989) 601
25) J.F. Beacom, R.N. Boyd, A. Mezzacappa, Phys. Rev. Lett. **85** (2000) 3568
26) D.E. Groom *et al.*, Eur. Phys. J. **C15** (2000) 1
27) R. Barate *et al.*, Eur. Phys. J. **C2** (1998) 395
28) A. Nucciotti *et al.*, Nucl. Instr. and Meth.**A444** (2000) 77
29) F. Gatti, Proc. of the Int. Conf. Neutrino 2000, Sudbury, Canada, Nucl.
Phys. **B** (Proc. Suppl.) **91** (2001), 293
30) G.L. Folgi *et al.*, hep-ph/0106247
31) H.V. Klapdor-Kleingrothaus, hep-ph/0103074
32) G. Beamson *et al.*, J. Phys. Sci. Instrum. Vol. 13 (1980) 64
33) R.G.H. Robertson *et al.*, Phys. Rev. Lett. **67** (1991) 957
34) E. Holzschuh *et al.*, Phys. Lett. **B287** (1992) 381
35) H. Kawakami *et al.*, Phys. Lett. **B256** (1991) 105
36) W. Stoeffl, D.J. Decman, Phys. Rev. Lett. **75** (1995) 3237
37) V.M. Lobashev *et al.*, Phys. Lett. **B460** (1999) 227
38) C. Weinheimer *et al.*, Phys. Lett. **B460** (1999) 219
39) V.M. Lobashev, Nucl. Inst. and Meth. **A240** (1985) 305
40) A. Picard *et al.*, Nucl. Inst. Meth. **B63** (1992) 345
41) L. Fleischmann *et al.*, J. Low Temp. Phys. **119** (2000) 615

42) L. Fleischmann *et al.*, Eur. Phys. J. **B16** (2000) 521
43) A.I. Belesev *et al.*, Phys. Lett. **B350** (1995) 263
44) V.M. Lobashev *et al.*, Proc. of the Int. Conf. Neutrino 2000, Sudbury, Canada, Nucl. Phys. **B** (Proc. Suppl.) **91** (2000) 280
45) H. Backe *et al.*, Proc. of Neutrino 96, Helsinki/Finland, June 1996, World Scientific/Singapure
46) V.N. Aseev *et al.*, Eur. Phys. J. **D10** (2000) 39
47) H. Barth *et al.*, Prog. Part. Nucl. Phys. **40** (1998) 353
48) B. Bornschein, PhD thesis, Mainz University, 2000
49) J. Bonn *et al.*, Proc. of the Int. Conf. Neutrino 2000, Sudbury, Canada, Nucl. Phys. **B**(Proc. Suppl.) **91** (2001), 273
50) J. Bonn *et al.*, Nucl. Instr. and Meth. **A421** (1999) 256
51) R.D. Penzhorn *et al.*, Fus. Eng. Design **49-50** (2000) 753
52) IMEC vzw B-3001 Leuven, Belgium, `http://www.imec.be`, *private communication*
53) J. Ciborowski *et al.*, Eur. Phys. J. **C8** (1999) 157
54) J. Stephenson *et al.*, Phys. Lett. **B440** (1998) 89
55) Study on the vacuum tank of the spectrometer by the company ACCEL/Bergisch Gladbach, Germany
56) A. Saenz *et al.*, Phys. Rev. Lett **84** (2000) 242
57) S. Jonsell *et al.*, Phys. Rev. **C60** (1999) 034601
58) R.G.H. Robertson and D.A. Knapp, Ann. Rev. Nucl. Part. Sci. **38** (1988) 185
59) W. Kolos *et al.*, Phys. Rev **A37** (1988) 2297
60) B. Bornschein *et al.*, *publication in preparation*
61) A. Picard *et al.*, Z. Physik **A342** (1992) 71
62) A. Saenz, Konstanz University, Germany, *private communication*
63) A. Kovalik, talk given at the preworkshop of the International Workshop on Neutrino Masses in the sub-eV Range, Bad Liebenzell/Germany, January 2001, (`http://www-ik1.fzk.de/tritium/liebenzell`)
64) O. Dragoun *et al.*, Nucl. Instr. Meth. **A365** (1995) 385
65) R.S. Van Dyck *et al.*, Phys. Rev. Lett. **70** (1993) 2888
66) W. Quint, talk given at the workshop of the International Workshop on Neutrino Masses in the sub-eV Range, Bad Liebenzell/Germany, January 2001, (`http://www-ik1.fzk.de/tritium/liebenzell`)
67) E.W. Otten, Prog. Part. Nucl. Phys. **32** (1994) 153
68) H.C. Sun *et al.*, CJNP **15** (1993) 261
69) V. Aseev *et al.*, *A next generation tritium beta decay experiment...*, `http://www-ik1.fzk.de/tritium/pubfig.html`